AD-A040 738 NAVAL RESEARCH LAB WASHINGTON D C F/G 9/5
SQUID ELF RECEIVING ANTENNA FOR SUBMARINE APPLICATIONS.(U)
MAY 77 R J DINGER, J R DAVIS, J A GOLDSTEIN

UNCLASSIFIED NRL-8118 NL

1 OF 1
AD A040738

END

DATE FILMED
7-77

NRL Report 8118

SQUID ELF Receiving Antenna for Submarine Applications: Final Report

ROBERT J. DINGER, JOHN R. DAVIS,
JOSEPH A. GOLDSTEIN, and WILLIAM D. MEYERS

Telecommunications Systems Technology Branch
Communications Sciences Division

MARTIN NISENOFF, STUART A. WOLF, and JAMES J. KENNEDY

Cryogenics and Superconductivity Branch
Material Sciences Division

May 25, 1977

NAVAL RESEARCH LABORATORY
Washington, D.C.

SECURITY CLASSIFICATION OF THIS PAGE (When Data Entered)

REPORT DOCUMENTATION PAGE

READ INSTRUCTIONS BEFORE COMPLETING FORM

1. REPORT NUMBER: NRL Report 8118	2. GOVT ACCESSION NO.
3. RECIPIENT'S CATALOG NUMBER	
4. TITLE (and Subtitle): SQUID ELF RECEIVING ANTENNA FOR SUBMARINE APPLICATIONS. FINAL REPORT	5. TYPE OF REPORT & PERIOD COVERED: Final report on one phase of an NRL problem
	6. PERFORMING ORG. REPORT NUMBER
7. AUTHOR(s): Robert J. Dinger, John R. Davis, Joseph A. Goldstein, William D. Meyers, Martin Nisenoff, Stuart A. Wolf, and James J. Kennedy	8. CONTRACT OR GRANT NUMBER(s)
9. PERFORMING ORGANIZATION NAME AND ADDRESS: Department of the Navy, Naval Research Laboratory, Washington, D.C. 20375	10. PROGRAM ELEMENT, PROJECT, TASK AREA & WORK UNIT NUMBERS: NRL Problem R07-34, XF21-222-035 62721N
11. CONTROLLING OFFICE NAME AND ADDRESS: Department of the Navy, Naval Electronic Systems Command, Washington, D.C. 20360	12. REPORT DATE: 25 May 1977
	13. NUMBER OF PAGES: 50
14. MONITORING AGENCY NAME & ADDRESS(if different from Controlling Office)	15. SECURITY CLASS. (of this report): Unclassified
	15a. DECLASSIFICATION/DOWNGRADING SCHEDULE
16. DISTRIBUTION STATEMENT (of this Report): Approved for public release; distribution ulimited.	
17. DISTRIBUTION STATEMENT (of the abstract entered in Block 20, if different from Report)	
18. SUPPLEMENTARY NOTES	
19. KEY WORDS (Continue on reverse side if necessary and identify by block number): Antennas; Extremely low frequencies; Receivers; Submarine antennas; Superconductors	

20. ABSTRACT (Continue on reverse side if necessary and identify by block number)

An ELF receiver using a triaxial array of superconducting quantum interference devices (SQUIDs) can provide an omnidirectional receiving capability unobtainable with conventional ELF antennas. The ELF SQUID receiver development program has undertaken (a) achievement of a prototype SQUID device with sufficient sensitivity, dynamic range, and linearity; (b) determination of the motion spectrum for a candidate receiver platform; (c) design of a motion processing technique to remove residual motion noise; and (d) provision of a suitable cryogenic environment. Two prototype SQUID antennas, one

(continued)

20.

using point-contact sensors and the other using thin-film sensors, were procured and tested. The noise level of the point-contact antenna was measured in a shielded room and found to be no greater than $1.9 \times 10^{-14} T/\sqrt{\text{Hz}}$. The point-contact antenna was placed on the ocean bottom at a depth of 100 m, and the broadcast ELF signal from the U.S. Navy's test transmitter was successfully received. The required platform stabilization was demonstrated in a towing basin by taking measurements of motion spectra on a hydrodynamically stabilized buoy designed to be towed by a submarine. Motion excursions within the ELF receiver bandwidth of 30-130 Hz were about 4×10^{-6} rad/$\sqrt{\text{Hz}}$; hence, motion-generated noise must be reduced further by about 88 dB. This remaining noise can be removed by an adaptive technique that processes the SQUID outputs. This technique was shown to work by processing the outputs (offline) of the SQUID antenna while the SQUID was being vibrated. The motion removal technique is sensitive only to the projection of the signal vector on the earth's magnetic field. This could lead to some degradation in performance in northern latitudes; however, this degradation can be recovered and the signal-to-noise ratio improved by decreasing the sensor intrinsic noise level. It is concluded that the feasibility of a SQUID ELF receiver has been demonstrated. However, several tasks remain before engineering development of an operational ELF receiver can begin. These tasks include motion noise suppression in real time, ocean tests of the stabilized buoy, and preliminary development and testing of an integral tow cable and vent line.

CONTENTS

SQUID ELF RECEIVING ANTENNA FOR SUBMARINE APPLICATIONS: FINAL REPORT

I. INTRODUCTION

The Navy's proposed extremely-low-frequency (ELF) strategic communication system is intended to permit reliable, secure, low-data-rate communications from a single transmitter in the United States to submarines at operational depth and at ranges of several thousand kilometers. The skin depth of ELF radio waves in seawater is tens of meters; hence radio waves in the band of interest (30 to 130 Hz) experience little attenuation in penetrating to substantial depths beneath the ocean surface. The required receiver sensitivity in this environment is approximately 200 dB below 1 $V/m\sqrt{Hz}$ ($10^{-14}\,T/\sqrt{Hz}$), a level of performance that can be achieved by currently available E-field trailing-wire antennas.

Minimizing operational constraints on submarines attempting to receive ELF messages requies providing them with an omnidirectional receiving capability. The E-field trailing wire, which is an elementary dipole, has a cosine-shaped azimuthal antenna pattern. Since it is not practical to design a transverse E-field sensor with adequate sensitivity to complement the trailing wire, an H-field antenna is necessary. However, the best demonstrated sensitivity for a conventional H-field loop antenna trailed at speeds of operational interest is far below the required value. Consequently, a program was begun in 1974 to investigate the feasibility of using a superconducting quantum interference device (SQUID) to provide both the required sensitivity and the necessary omnidirectionality.

A number of reports and papers [1-9] describe the engineering questions that must be answered to establish feasibility and present some of the early results of measurements and tests on program-developed hardware. This is the final report on the SQUID ELF exploratory development. It summarizes briefly test results given in earlier reports, describes in detail the results of previously unreported measurements and tests, and presents conclusions and recommendations for future work.

We believe our results have demonstrated the feasibility of using a triaxial array of SQUID sensors as an ELF submarine receiver. A horizontally oriented dewar, necessary to cool the SQUID sensors, was shown to have a 102-day hold time. A candidate antenna platform—a hydrodynamically stabilized buoy—demonstrated a motion excursion level of a low enough amplitude that motion noise could be suppressed to below the required system noise level by a relatively simple electronic processing technique. Two prototype SQUID antennas were procured and evaluated, and both satisfied all ELF receiver requirements. One of these antennas received the broadcast ELF signal at a depth of 100 m in the ocean.

Manuscript submitted March 17, 1977.

Several tasks, however, remain before full-scale engineering development of an operational ELF receiver can begin. These include measurement of submarine-emitted ELF noise, implementation of the motion-noise suppression technique in real time, ocean testing of the stabilized buoy, and preliminary development and testing of an integral tow cable and vent line.

Section II of this report summarizes the previously reported work. Section III discusses two prototype SQUID antennas and describes various measurements and tests that have been conducted on them. Section IV discusses a series of underwater reception measurements in which a SQUID antenna was placed on the ocean bottom and the test ELF signal was received. Section V presents the results of a test in which the SQUID antenna was vibrated in the Earth's field and the motion-generated noise was reduced by using an adaptive motion processing technique. Section VI states our conclusions and gives recommendations for continuing development of a SQUID ELF receiver.

II. BACKGROUND AND SUMMARY OF PREVIOUSLY REPORTED WORK

A. Overview

Four broadly defined research and engineering areas were identified at the beginning of the program:

- Provision of the necessary cryogenic environment for cooling the SQUID sensors
- Specification, design, construction, and testing of a prototype SQUID antenna
- Determination of the motion spectrum for a possible SQUID antenna host platform
- Development and testing of a signal processing technique to reduce motion-generated noise to an acceptable level.

These four areas were addressed simultaneously throughout the duration of the program. Logically, however, specification and procurement of the prototype SQUID antenna should follow both the determination of the platform motion spectrum and development of the motion noise processing technique, since these determine in part the performance required of the SQUID antenna. Procurement and testing of the SQUID antenna was such a lengthy process that specification of the SQUID antenna requirements was of necessity one of the first steps in the program. Hence, we were forced to make intelligent *estimates* of such prototype SQUID parameters as pickup coil orthogonality, linearity, and dynamic range before we had definitive measurements. The SQUID parameters specified on the basis of incomplete data were quite adequate; in the case of pick-up coil orthogonality, the specification was actually more stringent than required.

Table 1 lists the milestones in the SQUID antenna development program. Items 1 through 7 in this table have been discussed in detail in the indicated references and are summarized in this section. Items 8 through 13 are discussed in detail in Secs. III, IV, and V.

B. Long-Hold-Time Dewar

Possible techniques for cooling the SQUID sensors to below a temperature of approximately 9 K (the superconducting transition temperature of niobium, the sensor material) were reviewed in Ref. 3. It was concluded that at the present state of cryogenic technology the simplest and most reliable cooling technique consists of mounting the SQUID antenna elements in a fiberglass dewar whose liquid helium hold time is at least 90 days, which is longer than the duration of a typical submarine deployment. To verify that a dewar could be constructed to provide this liquid helium hold time, and with dimensions and a shape that enable it to fit into a typical towed buoy, an experimental long-hold-time dewar was procured and evaluated.

A description of the dewar and a discussion of the various tests conducted with the dewar are given in Ref. 4. Table 2 summarizes the physical characteristics of the dewar and gives results of the hold-time test. Although the measured hold time of 102 days exceeds the 90-day design goal for this dewar by 12 days, two points should be emphasized:

1. The hold-time test was conducted on a stationary dewar. Constant agitation of the liquid helium by the motion of the host platform can be expected to increase the boil-off rate and decrease hold time.

2. A triaxial SQUID sensor was not installed in the sensor chamber of the dewar during the hold-time test. This sensor will impose an additional heat load on the dewar and will decrease the hold time when in place.

Neither of these items is expected to decrease the hold time below 90 days.

C. Towed Buoy Motion Stability Tests

The motion of the buoy in the Earth's magnetic field will be a source of noise, since the SQUID is a vector sensor. Motion-induced variations that occur within the ELF receiver bandwidth of 30 to 130 Hz will be a major source of noise and must be removed by suitable signal processing. In addition, the motion-induced noise must be low enough that the dynamic range of the SQUID output electronics will not be exceeded. That is, the full-scale output of the SQUID sensors must be large enough relative to the required system noise level that the largest motion-induced variations will not saturate the SQUID electronics.

To determine the system parameters influenced by motion of the buoy, we compiled motion spectra on a towed buoy that was generally considered to be the most hydrodynamically stable communications buoy designed to date. This buoy [10], designed and constructed in 1972 by the David W. Taylor Naval Ship Research and Development Center (DTNSRDC), was towed in the 650-m-long towing basin at DTNSRDC at speeds between 2 and 7 knots. The buoy was instrumented with rate gyroscopes and accelerometers whose outputs were recorded on magnetic tape.

The data taken during these tests and their interpretation have been given in Refs. 5 and 6. The results can be summarized as follows:

Table 1—Chronology of Milestones in the SQUID Antenna Development Program

Milestone	Reference	Date
1. Study of possible cooling techniques completed	3	Sept. 1974
2. Specifications issued for prototype SQUID antenna	7, 8	Oct. 1974
3. Motion stability tests of stabilized towed buoy conducted at NSRDC	5, 6	Nov. 1974
4. Long-hold-time dewar received	4	May 1975
5. SHE* SQUID antenna received	7, 8	May 1975
6. Surface reception measurements conducted with SHE antenna	7, 8	Aug. 1975
7. Long-hold-time dewar test successfully completed	4	Sept. 1975
8. SHE antenna coil orthogonality measured at NASA-Goddard	—	Oct. 1975
9. Noise measurements of SHE antenna conducted in shielded room at National Magnet Lab	—	Jan. 1976
10. Underwater reception measurements conducted at San Clemente Island, Calif.	—	Mar.-Apr. 1976
11. Develco SQUID antenna received	—	June 1976
12. Reception and comparison measurements of SHE and Develco SQUID antennas conducted	—	Aug. 1976
13. SQUID outputs recorded during motion in Earth's field	—	Aug. 1976

*Superconductivity Helium Electronics Corp., San Diego. Calif.

Table 2—Summary of Long-Hold-Time Dewar Characteristics

Parameters	Measurement
Physical	
Size	0.56-m diameter
	1.83-m length
Material	G-10 fiberglass
Liquid helium volume	180 l
Weight	190 kg empty
	209 kg full
Manufacturer	ScT, Inc.
	Mountain View, Calif.
Performance	
Measured hold time	102 days
Average boil-off rate	1.8 l/day
Frequency response	d.c. to 300 Hz

1. Low-frequency oscillations of the towed buoy that occur below frequencies of 4 Hz have a maximum amplitude of approximately 3×10^{-3} rad/$\sqrt{\text{Hz}}$. This implies that the SQUID sensors must have a dynamic range of 143 dB.

2. With properly faired hydrofoil trailing edges, the motion amplitude within the 30-130 Hz receiver bandwidth can be maintained at a level of 4×10^{-6} rad/$\sqrt{\text{Hz}}$ or less. As discussed in Sec. II.D, this angular excursion results in motion-related noise 86 dB above the required receiver sensitivity.

3. The prominent spectral features are relatively independent of buoy speed up to the maximum testing speed of 7 knots, which is the maximum design speed of this buoy. It should be a straightforward matter to adapt this design to higher speeds and maintain the angular excursion levels measured at 7 knots. Care must be taken in design to avoid inducing wake instabilities at higher speeds, which may cause the buoy to oscillate.

D. Motion Noise Processing

The buoy motion stability tests described in Sec. II.C demonstrated that within the processing bandwidth of 30-130 Hz the motion excursions were no greater than 4×10^{-6} rad/$\sqrt{\text{Hz}}$. In simplified form, the signal induced in a SQUID sensor rotated through an angle Ω in the Earth's magnetic field $\mathbf{H}_e$ from an initial orientation θ_0 of the sensor axis relative to $\mathbf{H}_e$ is given by

$$H_m = H_e[\cos\theta_0(\cos\Omega - 1) + \sin\theta_0 \sin\Omega]. \tag{1}$$

For $\Omega = 4 \times 10^{-6}$ rad/$\sqrt{\text{Hz}}$ and $\theta_0 = 90°$ (the worst case), $H_m = 2 \times 10^{-10} T/\sqrt{\text{Hz}}$. This motion-induced noise, which is 86 dB greater than the required $10^{-14} T\sqrt{\text{Hz}}$ noise level of the receiver, must be removed by processing the SQUID outputs.

The technique developed to remove this motion noise has been thoroughly discussed in Refs. 7-9. These references derive the equation for the technique and discuss the results of a computer simulation. Section V of this report describes an experment in which the SQUID antenna was placed on an oscillating platform and its outputs were recorded while it underwent motion. These recorded outputs were then processed by our motion-noise processing technique. In this section, the equation for the motion-removal technique and the conclusions of the simulation experiments are summarized in enough detail to aid understanding of the tests described in Sec. V.

Let $\mathbf{V} = (V_1, V_2, V_3)$ represent the output of the three SQUID sensors that are nearly orthogonal. Assume that at some time $t = 0$, which is the beginning of the processing, the three SQUID outputs are simultaneously set equal to zero, so that subsequent sensor outputs are measured with respect to the values at $t = 0$. References 8 and 9 demonstrate that a quantity S, defined by

$$S = 2\mathbf{A} \cdot \mathbf{V} + \mathbf{V}^2, \tag{2}$$

can be formed so that motion noise is greatly suppressed. In Eq. (2), $\mathbf{A}$ is a vector approximately equal to Earth's field vector $\mathbf{H}_e$. Equation (2) is valid for sensors whose pickup loops are orthogonal to within approximately 10^{-3} rad and whose magnetic-field-to-voltage scale factors are matched to within 1 part in 10^3. The quantity S is in turn equal to

$$S = 2\mathbf{H}_e \cdot (\mathbf{H}_s + \mathbf{H}_n) \tag{3}$$

where $\mathbf{H}_s$ = ELF signal vector and $\mathbf{H}_n$ = atmospheric noise. That is, S is proportional to the projection of $\mathbf{H}_s$ and $\mathbf{H}_n$ onto Earth's field but is independent of motion. The goal of the motion-noise removal technique is to determine $\mathbf{A}$ rapidly and accurately.

Equations (2) and (3) can be given a geometrical interpretation that will prove useful in discussing the experimental measurements of Sec. V. In a coordinate system whose axes are V_1, V_2, and V_3 (the three SQUID outputs), Eq. (2) is the equation of a sphere with a center at

$$X_0 = (-A_1, -A_2, -A_3) \tag{4}$$

and with a radius of

$$R^2 = (S + A_1^2 + A_2^2 + A_3^2).* \tag{5}$$

Equation (3) indicates that when $\mathbf{H}_s$ is removed by filtering, then $S = 2\mathbf{H}_e \cdot \mathbf{H}_n$. In this case, then,

$$R^2 \approx (2\mathbf{H}_e \cdot \mathbf{H}_n + A_1^2 + A_2^2 + A_3^2). \tag{6}$$

The term containing $\mathbf{H}_n$ in Eq. (6) is a fluctuation noise term whose *average* value is zero. Hence, the time-averaged value of R is given by

$$\langle R^2 \rangle = A_1^2 + A_2^2 + A_3^2 \tag{7}$$

where the average time is long enough to average ELF noise in a 30- to 130-Hz bandwidth, but short enough that possible changes in A_i due to large variations in the Earth's magnetic field are not included in the average. Comparing Eqs. (7) and (4), we see that the surface of the sphere passes through the origin. Figure 1 is a diagram of the sphere. The effect of $\mathbf{H}_n$ is shown in Fig. 1 as a fuzziness of the surface of the sphere. Also shown is the area of the sphere sampled by the SQUID outputs during the motion of the SQUID antenna. This sampled area is a very small fraction of the total area of the

*This can be shown by adding A_1^2, A_2^2, and A_3^2 to both sides of Eq. (2) to obtain

$$(V_1 + A_1)^2 + (V_2 + A_2)^2 + (V_3 + A_3)^2 = S + A_1^2 + A_2^2 + A_3^2,$$

which is compared with the standard equation for a sphere, given by

$$(x - x_0)^2 + (y - y_0)^2 + (z - z_0)^2 = R^2$$

where (x_0, y_0, z_0) = center coordinates and R = radius.

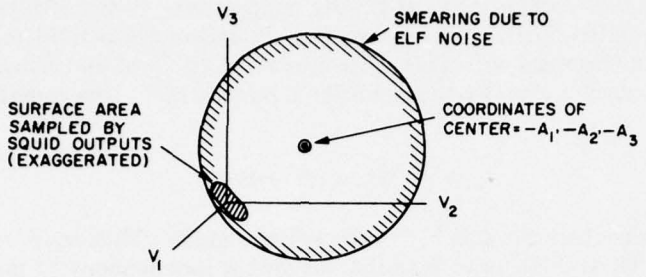

Fig. 1—Geometrical interpretation of Eq. (2)

sphere, since the full-scale output of each SQUID is $\pm 10^{-7} T$ compared to a sphere radius of $5 \times 10^{-5} T$. In this geometrical interpretation, the motion removal technique uses the points near the origin to determine the center of the sphere from the curvature of that area.

It is clear intuitively that the center of the sphere can be determined with the highest accuracy when the largest possible area of the sphere is sampled. For this reason the SQUID outputs must be filtered so that the inputs to the processing that determines the components of $\mathbf{A}$ contain large-amplitude motion variations. The towed buoy motion spectrum measurements (Sec. II.C) demonstrated that the largest variations occurred at frequencies between 1.0 and 4.0 Hz. These considerations lead to the processing technique shown in Fig. 2. The SQUID outputs are divided into two frequency domains by filtering. The low-pass filter outputs, which contain the large-amplitude motion-induced fluctuations are the inputs to the adaptive algorithm that determines the vector $\mathbf{A}$. The components of $\mathbf{A}$ are then combined with the high-pass filtered SQUID outputs according to Eq. (2) to produce an output, S given by Eq. (3), that is proportional to $\mathbf{H}_s$ and free of motion noise.

Two techniques have been developed for evaluating $\mathbf{A}$. The first is a least-squares method that minimizes the error given by

$$\epsilon = \sum_{j=1}^{N} [2\mathbf{A} \cdot \mathbf{V}(j) + \mathbf{V}^2(j)]^2 \tag{8}$$

where $\mathbf{V}(j)$ denotes a signal sample taken at the jth sampling time and N is the number of samples. The solution for $\mathbf{A}$ in terms of the sampled values of $\mathbf{V}(j)$ is given in Refs. 8 and 9.

The second technique uses a steepest descent algorithm that updates the current value of $\mathbf{A}_{\text{old}}$ according to an equation of the form

$$\mathbf{A}_{\text{new}} = \mathbf{A}_{\text{old}} - K \Delta_A \xi, \tag{9}$$

where K is a constant and ξ is a generalized error function. In our work, an error function given by

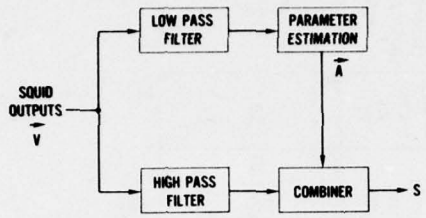

Fig. 2—Motion processing technique

$$\xi = \int_{t}^{t+T} S^2 dt \tag{10}$$

was used. The constant K controls the rate at which the minimum value of $\mathbf{A}$ is approached. An initial value of $\mathbf{A}$ must be supplied to begin the process.

These techniques were simulated on a digital computer. The simulated SQUID outputs were obtained by integrating the rate gyroscope signals recorded during the buoy motion stability tests described in Sec. II.C. This output, proportional to buoy angular excursion, was then combined with assumed values of the Earth's magnetic field to produce the simulated SQUID output. In this manner the simulated SQUID signals relfected the amplitude and frequency content of SQUIDs that would actually have been mounted on the towed buoy. The simulation results demonstrated in general that both the least-squares and steepest descent techniques are capable of evaluating $\mathbf{A}$ to the necessary degree of accuracy.

III. PROTOTYPE SQUID ANTENNAS

A. Description of Systems

The original intent was to purchase a single three-axis SQUID magnetometer system for evaluation of the SQUID ELF H-field antenna concept. However, in the proposals received from SQUID manufacturers, two distinct design concepts evolved and thus two systems were purchased so that the performance of each could be evaluated. Table 3 lists the specifications for the antennas and gives the measured performance of each.

1. Point-Contact SQUID System

One system, built by the SHE Corporation of San Diego, Calif., used a bulk toroidal niobium SQUID sensor with a "permanently" adjusted point contact [11]. This type of sensor had just become commercially available, and there was very little data on its reliability under field conditions. However, preliminary tests in the laboratory indicated that the performance of this type of sensor was at least comparable to that of the thin-film SQUID sensor, available commercially for several years.

Table 3—Specified and Measured Parameters for the SQUID Antennas

	Manufacturer	Date Received	Noise Level ($10^{-12} T/\sqrt{Hz}$)	*Sensor Orthogonality*		Dynamic Range (dB)	Frequency Response* (Hz)	Linearity (dB)	Scale Factor ($V/10^{-6} T$)	Dewar Size† (cm)	Dewar Capacity (l)	Operating Hold Time (days)
				Mechanical (10^{-3} rad)	Magnetic (10^{-3} rad)							
Specified	—	May 1975	10^{-2}	(‡)	0.1	140	d.c.-130	140	(‡)	(‡)	(‡)	7
Measured												
Antenna 1	SHE Corp.	May 1975	$<1.1 \times 10^{-2}$ §	0.07#	< 0.2**	139††	d.c.-130#	140#,‡‡	±90.9**	30.5 × 130	20	>7
Antenna 2	Develco, Inc.	June 1976	10^{-2}#,§§	<0.1	(§§)	143††	d.c.-130#	130#,##	±66.7#,§§	25 × 120	15	>7

*Flat within stated interval to ±0.5 dB.
†Diameter × height.
‡Not specified.
§Measured in shielded room.
#Measured at contractor's facility.
**Measured in precision Braunbek coil system.
††Computed from noise level and scale factor.
‡‡Ratio of maximum deviation of output at d.c. from best straight line.
§§Test could not be performed by NRL personnel because of late delivery. All specifications refer to the antennas in the increased-sensitivity mode (nominal noise level = $10^{-14} T/\sqrt{Hz}$) rather than the reduced-sensitivity mode (nominal noise level = $10^{-13} T/\sqrt{Hz}$).
##Ratio of third-order intermodulation product amplitude to test signal amplitude.

In the SHE system, the RF bias circuitry was located at the top of the dewar, and coaxial transmission lines connected it to the SQUID sensor located in the liquid helium reservoir. (See Fig. 3.) A 100-m cable connected the electronics at the dewar top to the control chassis that contained the feedback circuitry, the output terminals for each of the channels, and the remote controls for adjusting and tuning the RF bias circuits. The interconnecting cable carried the detected RF signal from the dewar to the control box, the processed feedback signal back to the dewar, and the control voltages used to time and adjust the RF circuits at the top of the dewar. The various leads in the interconnecting cables had to be shielded very carefully to reduce possible interferences among the various sets of leads in the cable from external noise sources.

The magnetic sensing coils for the three SQUID channels were wound on a quartz cube. The cube, approximately 8 cm on an edge, was ground and polished with adjacent faces orthogonal to one another to within less than 10^{-4} rad. Grooves to accept the pickup coils were ground into the quartz block midway between each set of parallel faces. When the niobium pickup coil was laid into a groove, the plane of the loop was parallel to the corresponding set of faces of the cube to within less than 1 part in 10^4. For maximum magnetic orthogonality between these coils all superconducting lead wires, superconducting shields, SQUIDs, etc., had to be positioned about a symmetry axis of the cube to ensure minimum mutual inductance between the coils. Inductance switches located in series with each pickup coil allowed the sensitivity of the sensors to be reduced from $10^{-14}\,T/\sqrt{\text{Hz}}$ to $10^{-13}\,T/\sqrt{\text{Hz}}$. This reduced-sensitivity mode was sometimes used during surface measurements.

Another distinguishing feature of the SHE system was that the feedback signal was injected in series into the flux transformer by means of a superconducting d.c. transformer, as shown in Fig. 4. Accordingly, when the feedback circuit was closed, the feedback signal maintained the current flowing in the flux transformer at zero, in both the primary sensing coil and the secondary coil coupling it to the SQUID sensor.

The SHE system proved an exceptionally rugged and field-worthy instrument. During the surface reception measurements described in Sec. III.C, an accident occurred. The antenna was toppled, pulled from its shelter, and dragged 10 m across the ground by a road grader whose blade had snagged the 100-m flexible cable. The antenna suffered no damage. Also, during the underwater reception measurements described in Sec. IV, numerous severe shocks were suffered without damage by the SHE antenna while being lowered and raised.

2. *Thin-Film SQUID System*

The second SQUID system, built by Develco, Inc., Mountain View, Calif., used thin-film SQUID sensors. This type of device is fabricated from a cylindrical thin film of an indium-tin alloy deposited on a quartz tube. At one point along the circumference of the film a very narrow constriction is sculptured. This type of sensor had been used in a large number of SQUID systems built during about three years prior to this procurement, and its characteristics were fairly well documented [12].

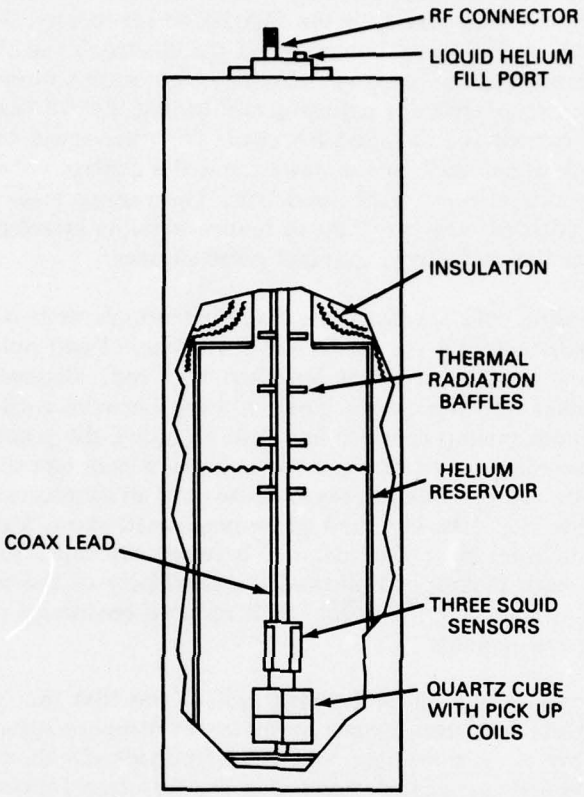

Fig. 3—Cutaway of SHE SQUID antenna. Only one of the three coaxial leads and RF connectors is shown.

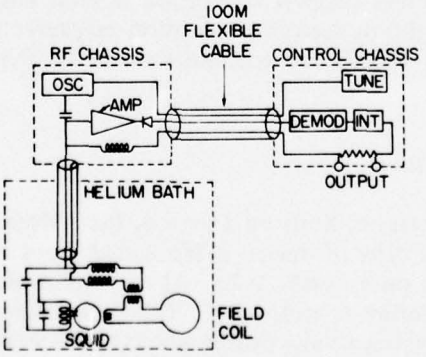

Fig. 4—Circuit for individual channel of SHE SQUID antenna

In the Develco system, both the RF bias and feedback circuitry were located at the top of the dewar, as shown in Fig. 5. A 100-m cable connected the electronics at the top of the dewar to a terminal box where the output signals from the three channels and voltage control leads for adjusting the RF bias circuitry were located. By placing the feedback circuitry at the dewar, possible pickup of external noise by the leads between the feedback circuitry and the dewar was minimized compared to the case of the SHE system, in which the feedback signal had to be transmitted down a 100-m interconnecting cable. (External pickup by the feedback leads of the SHE system was never a problem, as these leads had been adequately shielded against external pickup.)

Develco proposed to use Helmholtz coils for the primaries of each of the three flux transformers. A quartz cube was ground and polished to a precision of better than one part in 10^4. A quartz disc was positioned at the center of each face of the cube and cemented in place. Niobium wires were wound around each of these discs and the loops on opposite faces were connected in series to form the primary of each flux transformer. The construction tolerences required to achieve a given degree of orthogonality among three sets of Helmholtz coils mounted on the faces of a cube are much less stringent than those for the same degree of orthogonality of three simple coils mounted on adjacent faces of the cube. As in the other system, great care had to be taken in positioning superconducting lead wires, superconducting shields, and SQUID assemblies to maintain symmetry along one axis of the cube and thus minimize mutual coupling among the set of pickup coils.

Another distinguishing feature if the Develco system was that the feedback signal was applied in to the secondary, and thus also to the primary, of the flux transformer. The sense of the feedback signal was such that when the feedback loop was closed the current flowing in the secondary was zero while the current in the primary of the flux transformer was twice the current that flowed into the primary when the feedback circuit was closed.

B. Evaluation of the SQUID Systems

It was intended at the outset of the program that both antennas would be procured simultaneously and then subjected to identical evaluation measurements. As indicated in Table 3, the SHE antenna was received on schedule, whereas the Develco antenna was not received until a year later, near the end of the program; hence, we could not conduct some of the tests on the Develco antenna. Table 3 indicates which ones could not be conducted. In addition to the acceptance tests conducted at the manufacturer's facility, three major tests were conducted after delivery of the antennas:

- Measurement of magnetic orthogonality of the pickup loops at the magnetic test facility of NASA's Goddard Space Flight Center, Greenbelt, Md.

- Measurement of the SQUID sensor noise level at the National Magnet Laboratory, Cambridge, Mass.

- Reception measurements to detect transmissions from the U. S. Navy's test ELF transmitter.

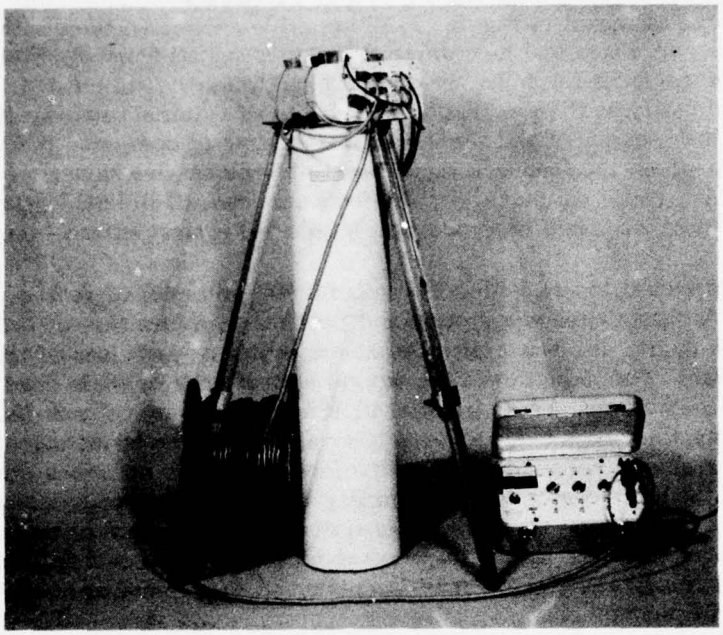

Fig. 5—Triaxial SQUID magnetometer system built by Develco, Inc.

A side-by-side comparison of the SHE and Develco antennas was possible only in the last test.

1. Measurement of Pickup Coil Orthogonality

The SHE SQUID magnetometer was taken to the Magnetic Test Facility of the Goddared Space Flight Center in Greenbelt, Md. The Goddard facility consists of three sets of 13-m-diameter, mutually orthogonal coils in a Braunbek configuration to maximize the field uniformity at the center of the system. This facility can null the Earth's magnetic field to at least $10^{-9}T$ and can provide magnetic fields in any direction varying from zero to $5.5 \times 10^{-5}T$ with an accuracy of $10^{-9}T$. The orthogonality of the Goddard facility was specified to be 10^{-4} rad, but the orthogonality of the coils has not been verified by experimental measurements.

The triaxial SQUID magentometer in the low-sensitivity ($10^{-13}T/\sqrt{\text{Hz}}$) mode was mounted at the center of the test area, and the flux transformer primaries were aligned to within 10^{-2} rad of the Goddard coils. The Earth's magnetic field was nulled, and a calibration field was applied to each axis to determine the scale factor of each channel of the SQUID magnetometer. The SQUID outputs were measured with a digital voltmeter, and several sets of readings (field on, field off, field reversed) were averaged to determine these scale factors accurately.

The following procedure was used to check the orthogonality of the SQUID sensing coils. With the SQUID axes alined within 10^{-2} rad of the Goddard coils, a field of $9 \times 10^{-6} T$ was applied in turn to each of the three perpendicular directions. For each application of a known field, the changes in the outputs of the SQUID axes orthogonal to the applied field direction were measured (e.g., for a vertical applied field, the east-west and north-south SQUID readings were noted before and after applying the field). The output of the SQUID whose coil was alined with the applied field could not be determined, since the field value along this axis exceeded the dynamic range of the sensor. It is conservatively estimated that this $9 \times 10^{-6} T$ field is accurate to about 0.01% for a 10^{-2}-rad alignement.

For convenience we will denote the three Goddard field directions by *NS*, *EW*, and *UD* and the directions of the three SQUID axes by x, y, and z. Initially x was alined with *NS*, y with *EW*, and z with *UD*. If the orthogonality errors in the SQUID axes are denoted by ϵ_{xy}, ϵ_{xz}, ϵ_{yz} and the orthogonality errors in the Goddard field directions are η_{NE}, η_{NU}, and η_{UE}, then it can be shown that for a $9 \times 10^{-6} T$ field applied in turn to *NS*, *EW*, and *UD* the following set of equations is valid to first order in ϵ and η:

$$\frac{H_x^N H_x^E + H_y^N H_y^E + H_z^N H_z^E}{81 \times 10^{-12}} = \eta_{NE} \pm \epsilon_{xy} \tag{11a}$$

$$\frac{H_x^N H_x^U + H_y^N H_y^U + H_z^N H_z^U}{81 \times 10^{-12}} = \eta_{NU} \pm \epsilon_{xz} \tag{11b}$$

$$\frac{H_x^E H_x^U + H_y^E H_y^U + H_z^E H_z^U}{81 \times 10^{-12}} = \eta_{EU} \pm \epsilon_{yz}. \tag{11c}$$

Here H_i^N, H_i^E, H_i^U ($i = x, y, z$) are the components of the fields applied in the *NS*, *EW*, and *UD* directions respectively. For example, H_x^N is the magnetic field sensed by the X-axis SQUID for the external field applied in the *NS* direction. The ± sign on the right-hand side of these equations arises from an ambiguity in the relative sense of the orthogonality errors in the SQUID axes and the Goddard coils. This ambiguity can be removed by rotating the SQUID axes by 90° in each of the three principal planes and repeating the measurement described above. After the measurements with x alined along *NS*, the SQUID antenna was rotated about a vertical axis to place x along *EW*. For this orientation, the relevant equations are similar to Eqs. (11), except that Eq. (11a) is replaced by

$$\frac{H_x^N H_x^E + H_y^N H_y^E + H_z^N H_z^E}{81 \times 10^{-12}} = \eta_{NE} \mp \epsilon_{xy} \tag{12}$$

which resembles Eq. (11a) except for the inverted plus/minus signs. Hence the magnitudes of η_{NE} and ϵ_{xy} can be separated. The results of these measurements are given in Tables 4 and 5. From the values of (η_{NE} and ϵ_{xy}), Eqs. (11) and (12) imply that $\eta_{NE} = 1.55 \times 10^{-4}$ rad and $\epsilon_{xy} = 0.95 \times 10^{-4}$ rad. The latter value indicates that the magnetic orthogonality of the SHE SQUID antenna is indeed within the 10^{-4}-rad specification in this plane.

Unfortunately, we could not interchange the other axes to determine the other misalinements unambiguously, since the dewar could not be placed on its side. However, the consistency of the values of ($\eta_{NU} \pm \epsilon_{xz}$) and ($\eta_{EU} \pm \epsilon_{yz}$), which are nearly independent of rotation, suggests that both the Goddard coils and the SQUID antenna pickup coils are orthogonal to within $\approx 10^{-4}$ rad.

2. *Measurement of SQUID Noise Level*

The intrinsic noise level of each SHE SQUID sensor had been measured during acceptance tests at the contractor's facility by placing the probe in a superconducting lead shield. This shield, when cooled through its superconducting transition temperature ($\approx 7K$), became diamagnetic and acted as an excellent shield against changes in applied field. These tests demonstrated that the sensor noise level was less than the required value of $10^{-14} T/\sqrt{\text{Hz}}$ over the d.c.-to-200-Hz bandwidth. However, it is possible that paramagnetic or ferromagnetic impurities in the dewar walls or in the dewar radiation shields might introduce noise that would exceed the $10^{-14} T/\sqrt{\text{Hz}}$ value. Hence, an accurate assessment of system noise level requires the probe *and dewar* to be within a shield during the noise measurements.

The only facility in the United States capable of shielding an object the size of the SHE dewar to a level of the order of $10^{-14} T/\sqrt{\text{Hz}}$ is the Low Field Facility at the National Magnet Laboratory, which is operated by the Massachusetts Institute of Technology. The shielded room is constructed of three layers of mumetal and two layers of aluminum, formed into a dodecahedron. It is capable of reducing the ambient magnetic field to a value of $2 \times 10^{-14} T/\sqrt{\text{Hz}}$ or less at selected frequencies in the band from d.c. to 200 Hz. The residual noise in the room is primarily caused by 60-Hz leakage and motion of the room in response to building vibration. The latter noise is a minimum from midnight to about 6 a.m.

The SHE SQUID system was suspended from the walls of the room to decouple it from vibrations of the floor. A series of noise spectrum measurements was taken in the early morning, when the room was at its quietest. Spot noise measurements across the frequency band from d.c. to 500 Hz were taken using a Princeton Applied Research (PAR) Model 124 lock-in detector as a 10% bandwidth voltmeter. The results of these measurements are shown in Table 6. The variability of the values, particularly at the lower frequencies, is caused by mechanical vibration resonances. These values were in good agreement with the room noise spectrum determined in a previous set of measurements by another superconducting magnetometer. Hence, the measured values are environmentally limited; i.e., they reflect the limitation of the shielded room rather than of the SQUID sensors. We conclude that the overall system noise level of the SHE SQUID antenna is no larger than $1.9 \times 10^{-14} T/\sqrt{\text{Hz}}$.

Table 4—Magnetic Fields Measured During SHE SQUID Coil Orthogonality Tests

SQUID Orientation	Orientation of 9×10^{-6}T Field	Measured SQUID Outputs (10^{-9}T)		
		X	Y	Z
X‖EW	NS	-67.1	-9000*	-9.21
	EW	-9000*	67.5	-7.45
	UD	-8.1	-6.8	9000*
X‖NS	NS	9000*	-4.7	28.9
	EW	2.4	-9000*	-0.6
	UD	-31.3	2.6	9000*

*Assumed values—see text.

Table 5—Values of Error Quantities of Eq. (11).

SQUID Orientation	Error Quantities (10^{-3} rad)		
	$\eta_{NE} \pm \epsilon_{xy}$	$\eta_{NU} \pm \epsilon_{xz}$	$\eta_{EU} \pm \epsilon_{yz}$
X‖EW	0.25	0.26	0.22
X‖NS	0.06	0.26	0.15

Table 6—Noise Level (in Units of $10^{-14} T/\sqrt{\text{Hz}}$) Measured for the SHE SQUID Antenna in a Shielded Room

Sensor Axis	Frequency (Hz)					
	5	19	29	34	76	500
X	1.74	2.2	7.87	3.0	1.7	1.24
Y	2.8	3.9	—	2.29	1.86	1.4
Z	2.4	3.4	—	3.4	1.85	1.3

Reception of the broadcast ELF signal from the U.S. Navy ELF Test transmitter requires that the SQUID antenna outputs and a reference signal generated by a frequency synthesizer be recorded for later analysis. There was a serious concern that capacitive coupling of the reference signal into the high-impedance portion of the SQUID circuitry might give a false indication of a received signal. To test for this leakage, we recorded the SQUID outputs in the shielded room along with a 76-Hz reference. Analysis by a coherent detection method, described in the next section, revealed that there was indeed leakage of the reference signal into the SQUID electronics. Most of the leakage signal could be eliminated by physically separating the SQUID electronics and the synthesizer producing the reference. The last trace of the leakage signal was eliminated by recording the reference at twice the signal frequency and subsequently using a frequency-divide-by-two circuit to generate a reference during analysis. These measurements were important for determining the optimum recording configuration for the surface and underwater reception tests.

C. Surface Reception Measurements

Reception of a CW test signal broadcast by the U.S. Navy ELF transmitter at Clam Lake, Wisc., was an important test of the SQUID antennas. Although such a test, when performed above the ocean surface, does not require tthe SQUID sensors to operate near their noise level, successful reception does require the system to be free of RFI and of spurious noise pulses that have been known to plague SQUID sensors and also to be able to operate under field conditions in the presence of wide temperature extremes, moisture, wind, etc.

The reception measurements were conducted at our Stump Neck, Md., field site, where a 2-m-diameter air-core loop antenna was available for comparison. The first measurements were made during August 1975, with only the SHE SQUID antenna installed at the field site. The results of this test, including a plot comparing the temporal behavior of the SQUID and air-loop 76-Hz received signals, are given in Refs. 7 and 8. Additional surface reception measurements were made in August 1976, in which both the SHE and Develco antennas were installed at the field site. In this report, only the results of the latter test are given.

Figure 6 is a block diagram of the data recording system. The frequency of the transmitted signal was 76 Hz; however, as indicated in Sec. III.B, the reference signal to be recorded for postdetection processing was twice the frequency of the transmitted signal. The outputs of the SQUID antennas and the air-loop system were recorded for 16 h, including 2 h prior to transmitter turn-on, 12 h of transmission, and 2 h after transmitter turn-off.

A block diagram of the apparatus used to recover the transmitted signal by coherent integration is shown in Fig. 7. The in-phase and quadrature components were summed as shown to remove the effects of phase differences between the transmitter and reference signals.

During these reception measurements, both antennas performed well. Neither displayed any sensitivity to changes in ambient temperature, although the SHE antenna required a silicon grease coating on the connectors joining the RF boxes to the dewar, to

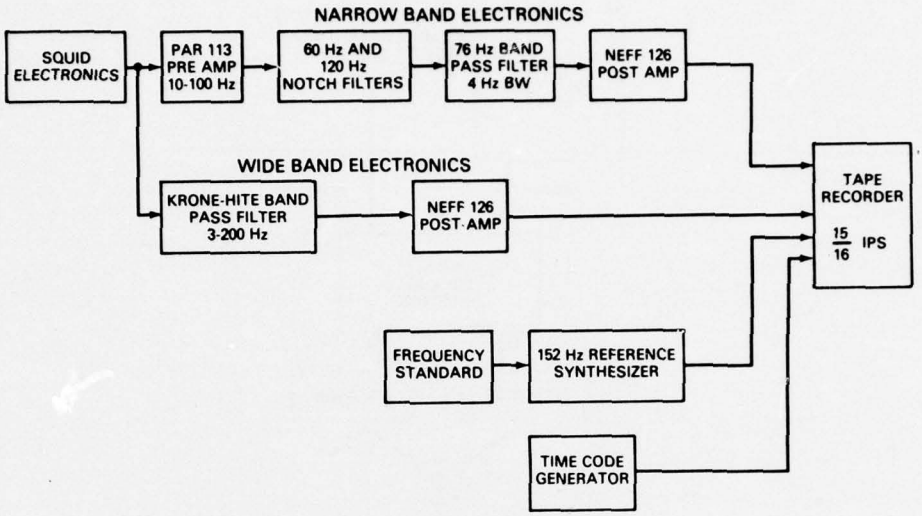

Fig. 6—Electronics used to record SQUID antenna outputs during surface reception measurements

prevent penetration of condensed moisture into this high-impedance portion of the SQUID circuit. In addition, atmospheric noise impulses were a problem because the rise time of the biggest impulses exceeded the slew rate of the SQUID antennas, causing the feedback loops to unlock and generate a d.c. shift ("flux jump") in the SQUID output. The effect of noise impulses, which were particularly bothersome in summer measurements, was eliminated by shielding the SHE antenna by a 0.8-mm-thick aluminum tube that provided an attenuation of 3 dB at 100 Hz. The Develco antenna was wrapped with multiple layers of aluminum foil to an approximate thickness of 0.8 mm.

Figure 8 is a graph of the coherently detected 76-Hz outputs of the two SQUID antennas and the loop antenna. The agreement of both SQUID antennas with the loop antenna is quite good. The approximately 2-dB constant difference in amplitude between the loop and the SQUID antennas is caused by the shielding surrounding the SQUID antennas, which attenuates a 76-Hz signal by approximately 2 dB. The Develco antenna agrees slightly better with the loop than does the SHE antenna, possibly because the alinement of the Develco antenna with the loop axis was superior.

D. Discussion

Overall, both the SHE and Develco antennas performed quite well. Both types of sensors (point-contact and thin-film), on the basis of the surface reception measurements, seem to be suitable for use in an ELF antenna. However, the Develco antenna at times displayed small discontinuous "jumps" or offsets in the SQUID outputs. The jumps had magnitudes that were usually no greater than several times the system noise level and hence could be seen only when the sensors were operated in a shielded environment. The jumps were caused by the motion of trapped magnetic flux in the thin film of the sensor

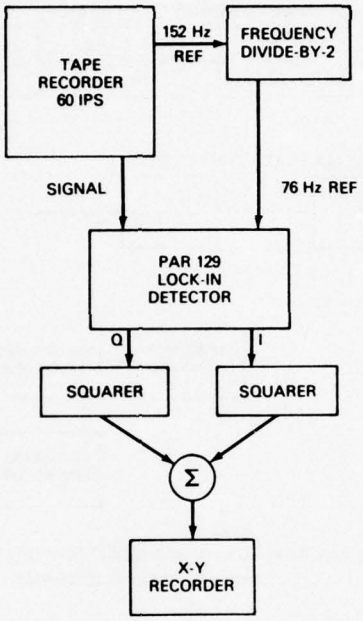

Fig. 7—Analysis equipment used to recover the transmitted signal during the surface reception measurements. "Q" indicates quadrature component, and "I" indicates in-phase component.

could be alleviated by periodically applying a heat pulse to the sensor to raise its temperature above the film's superconducting transition temperature. This heat pulse purged the thin film of trapped magnetic flux. The Develco system was equipped with a circuit that allowed a heat pulse to be applied manually to the sensor. The added complication of this circuit weighs against the use of the Develco type of thin-film sensors.

The Develco system configuration, in which both the RF bias and feedback circuitry are located at the top of the dewar, is preferable to that of the SHE configuration, in which they are separated. The Develco configuration, if implemented in a towed buoy, would allow a much longer tow cable, whose length would be limited only by such considerations as signal attenuation and induced noise. The SHE configuration, however, restricts the tow cable length to about 100 m because of excessive phase shift of the feedback signal. In summary, the optimum SQUID antenna configuration consists of point-contact SQUIDs with RF and feedback circuitry collocated at the dewar.

IV. UNDERWATER RECEPTION MEASUREMENTS

During March and April 1976, the SHE SQUID antenna was taken to San Clemente Island (SCI), Calif., for a series of underwater reception measurements. These

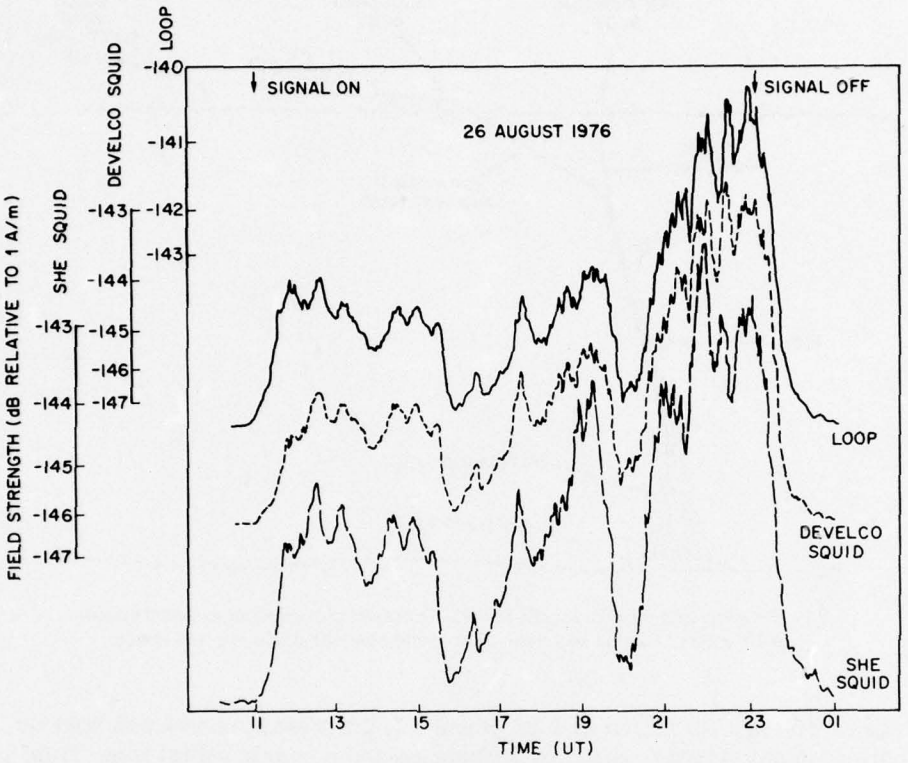

Fig. 8—Comparison of transmitted ELF signals as received on the two SQUID antennas and on a convential air-core loop antenna. Traces are offset vertically for displayed purposes.

measurements had two goals: (a) to demonstrate the low-noise performance level of the SQUID sensors by receiving the ELF signal at a depth where the noise level is determined by sensor noise and not atmospheric noise, and (b) to demonstrate that the SQUID antenna can be used in the hostile ocean environment. The SCI facility, which is operated by the Naval Ocean Systems Center (NOSC), San Diego, was an ideal location for the underwater measurements because a depth of 100 m was possible within 400 m of shore, operations could be carried out in winter due to the benevolent climate, and complete support facilities and personnel were available.

The operating configuration for the tests is shown in Fig. 9. The boat was an anti-submarine net tender about 20 m in length that has been converted to miscellaneous research purposes by NOSC. The SHE SQUID antenna control electronics and all recording and analysis electronics were located in a hut near the stern of the boat (Fig. 10). The boat was held in place at the test site by a three-point mooring; all anchors, chains, and cables associated with the mooring were kept at least 75 m from the SQUID antenna. The SHE SQUID antenna, dewar, and RF electronics were mounted in a fiberglass pressure vessel and joined to the boat electronics by a 200-m underwater cable. The pressure vessel (Fig. 11) was constructed of 1.25-cm-thick spun fiberglass and had a test

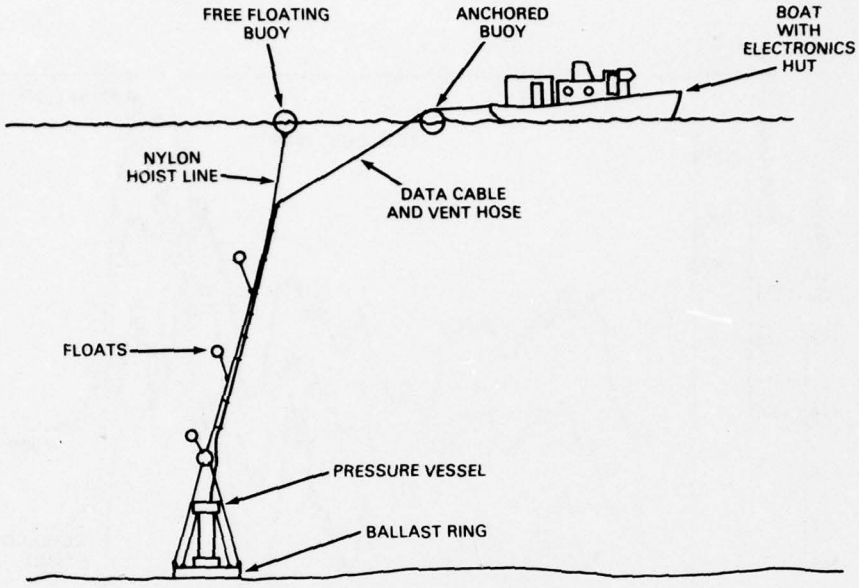

Fig. 9—Operating configuration for the underwater reception measurements (not to scale). Chains and cables for anchoring the buoy are not shown.

test depth of 150 m. As shown in Figs. 9 and 11, the pressure vessel was held on the ocean bottom in an upright position by a fiberglass and concrete ballast ring. Total submerged weight of the SQUID antenna/pressure vessel/ballast ring assembly was approximately 1600 kg.

Attached to the ballast ring and visible in Fig. 11 is an aluminum table that carried a compass and a television camera mounted on a pan-and-tilt head. Two tilt meters are also visible in Fig. 11. During emplacement on the bottom, the TV camera and its platform were attached to the ballast ring and connected to a monitor located on the boat by a second underwater cable, the reel for which is visible on the stern of the boat in Fig. 10. The pan-and-tilt head allowed the camera to view the compass, the tilt meters, the pressure vessel, and the vessel, and the ocean bottom during descent and after emplacement. In this manner the final orientation of the SQUID antenna and the condition of the bottom could be determined. Following emplacement the aluminum table was removed from the ballast ring by reeling in the TV monitor cable. The actual lowering of the ballast ring with the SQUID antenna was accomplished from a work barge with a crane and hoist. The orientation and attitude of the system on the bottom could not be selected or controlled; we had to accept the position that the system assumed on the bottom.

Venting of the helium gas evolved from the boiling liquid helium was accomplished through a nylon vent tube with a 0.95-cm ID and a 1.25-cm OD. This tube was rigid enough to withstand the 8.6-bar hydrostatic pressure at a depth of 100 m, but yet was

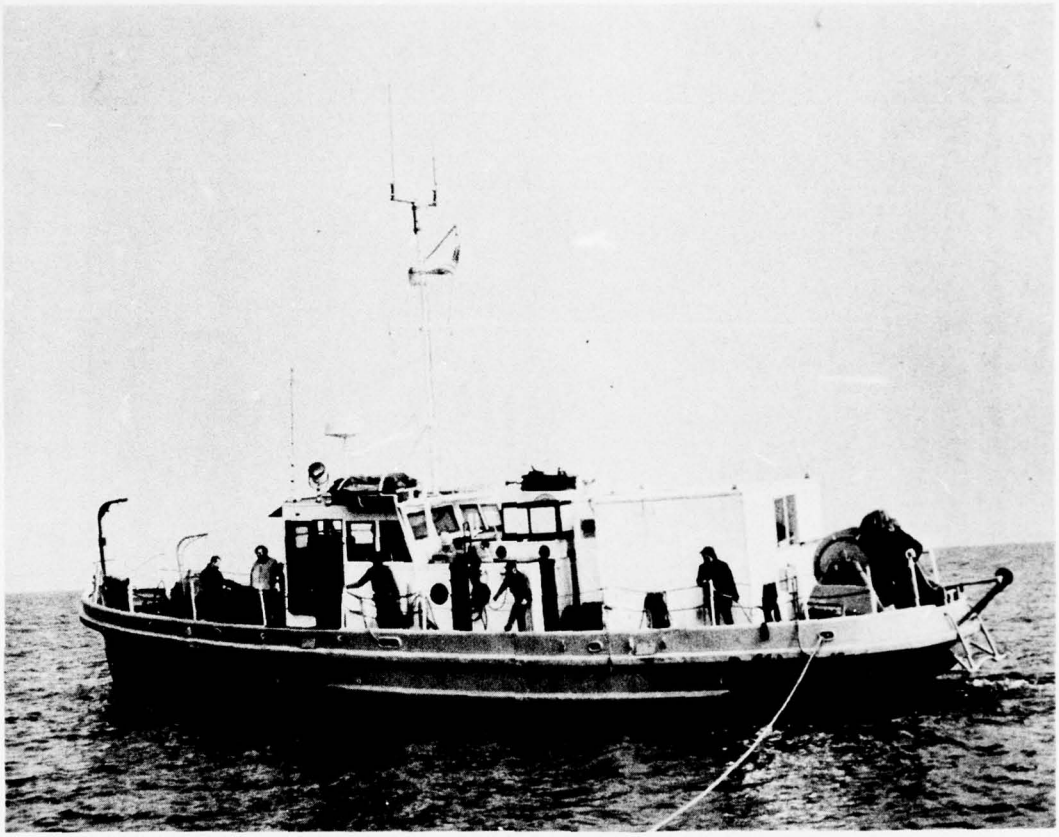

Fig. 10—Boat on which recording and processing electronics were mounted during underwater reception measurements

flexible enough to follow the contours of the control cable. A stainless steel check valve, attached at the top of the pressure vessel, was used to prevent flooding of the pressure vessel interior in the event of a ruptured vent line.

Two air-core ELF loop antennas were installed on San Clemente Island to serve as a surface reference for the SQUID antenna. The outputs of the loops, which were oriented to measure the radial and transverse components of the transmitted ELF signal, were recorded on a tape recorder along with a timing signal. Power for the land station was supplied by a propane motor generator.

Many problems were encountered during the tests, but eventually they were overcome to allow reception of the ELF signal. The problems included ground loops caused by intermittent short and open circuits in portions of the boat wiring, delays caused by a windstorm, an underwater cable that became filled with water because of cuts in the cable jacket suffered during the windstorm, and various difficulties associated with the mooring. Approximately two days of acceptable reception of the ELF signal were eventually obtained.

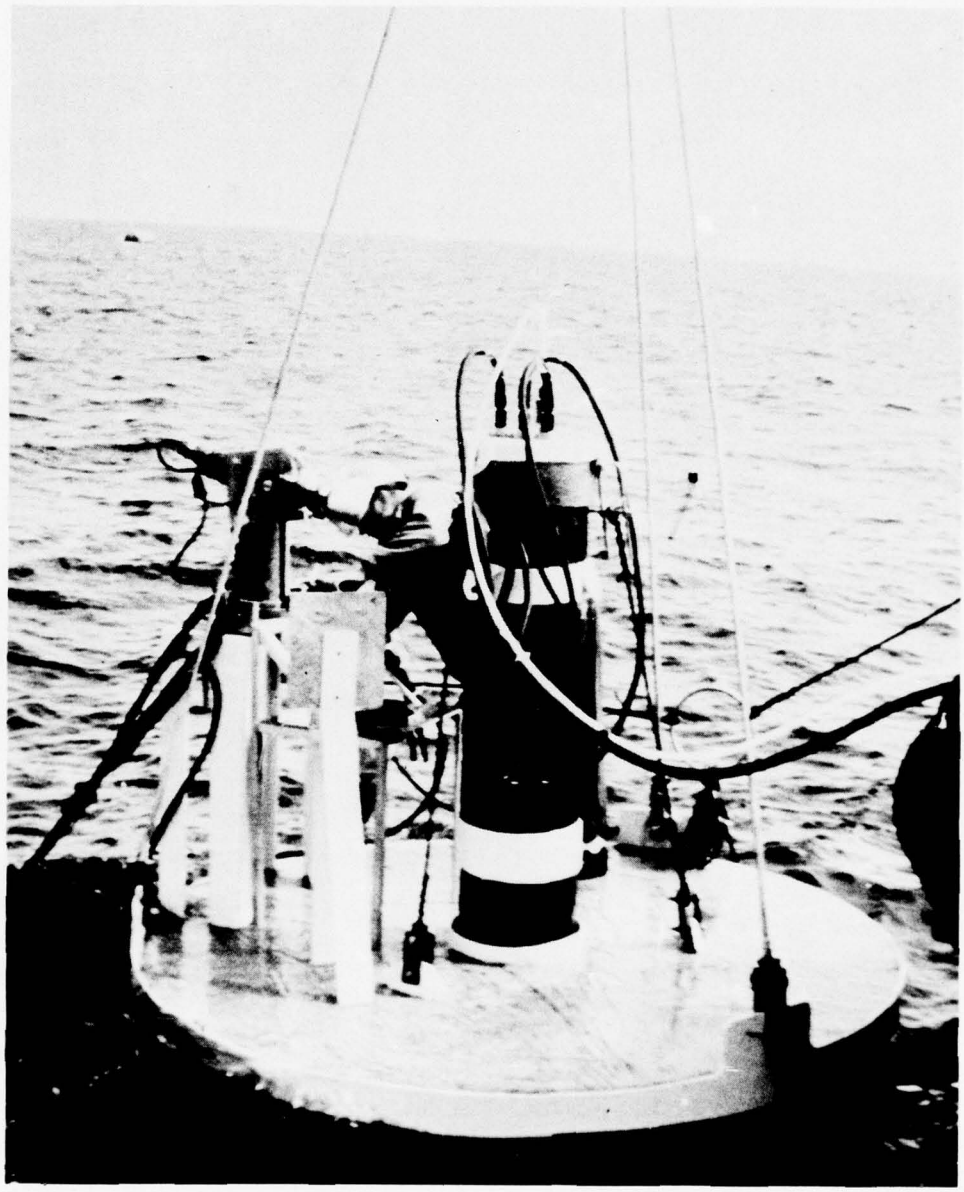

Fig. 11—Ballast ring with pressure vessel

Interpretation of the temporal variation in the SQUID-detected signal and comparison with the surface loop-detected signal are hampered by two factors. First, the underwater assembly oriented itself so that the horizontal SQUID axes were oriented approximately 35° from the axes of land-based loops; neither SQUID axis was oriented to measure the optimum vectorial component of the ELF signal. The result was a detected signal that, in addition to being closer to the system noise level than the surface loop detected signal, is a mixture of the azimuthal and radial propagating wave components. Hence, the loop-detected and SQUID-detected signals should not be expected to compare feature for feature. The second factor is the presence of interfering boat-generated noise in the SQUID output. Figure 12 is a time-frequency spectrum display of the Y-axis SQUID output. On this display a strong spectral line at 60 Hz has been removed by a notch filter. The prominent line at 39.5 Hz is apparently due to interference caused by the generator on the boat. The first harmonic of this interference at 79 Hz at times had sufficient spectral extent to interfere with coherent detection at 76 Hz.

Figure 13 is a graph of the 76-Hz coherently detected Y-oriented SQUID signal measured on Apr. 13, 1976. Figure 14 is a similar graph for the azimuthal component of the land station. The effective bandwidth in both figures is 2.6×10^{-4} Hz. Two features of the SQUID are puzzling. The first is the slow rate, compared to the land station, at which it increases in amplitude following transmitter turn-on; and the second its failure to return to zero following transmitter turn-off. We believe the apparently slow turn-on rate is real and does not compare with that of the surface loop because the Y-SQUID is not oriented in the optimum azimuthal direction; hence, the detected signal is lower and has a poorer signal-to-noise ratio. Failure of the signal to return to zero following transmitter turn-off can be explained by reference to Fig. 12, which displays the frequency spectrum of the Y-SQUID output from 0600 UT to 1200 UT. At approximately 1100 UT a series of large noise impulses began. They show on Fig. 12 as broadband noise covering the entire 0 to 100-Hz range. These large noise impulses, whose origin is uncertain, produced overloading of the lock-in detector. We believe that the signal would have followed the dashed line in Fig. 13 had it not been for the disturbances at 1100 UT. Other features of the Y-oriented SQUID sensor and the azimuthal loop compare fairly well. Both signals have a minimum between 0200 UT and 0400 UT, have a maximum near 0500 UT, and then begin to decrease. However, the SQUID sensor shows a steady increase until transmitter turn-off at 1000 UT, whereas the loop decreases until turn-off. The increase in the SQUID signal might be due partially to the influence of the radial component but is more likely due to an overall increase in system noise, which can be seen in Fig. 12 to occur near 0730 UT.

The mean signal level measured at the ocean surface between 0440 UT and 0500 UT is -141.2 dBH, and for the Y-oriented SQUID sensor it is -172.5 dBH. Correcting the SQUID sensor value to account for the 35° misalinement by adding +1.7 dB [= 20 log (cos 35°)] yields a value of -170.8 dBH as the measured value at a depth of 95 m and a difference between the surface and undersea values of 29.6 dB. The attenuation in seawater with a conductivity of 4 mho/m is 0.29 dB/m [13], yielding a theoretical difference of 27.5 dB. This value is in good agreement with the experimental difference, in view of the uncertainties in such quantities as depth (± 5 m), angular orientation (± 20°), and uncertain effect of boat-generated noise.

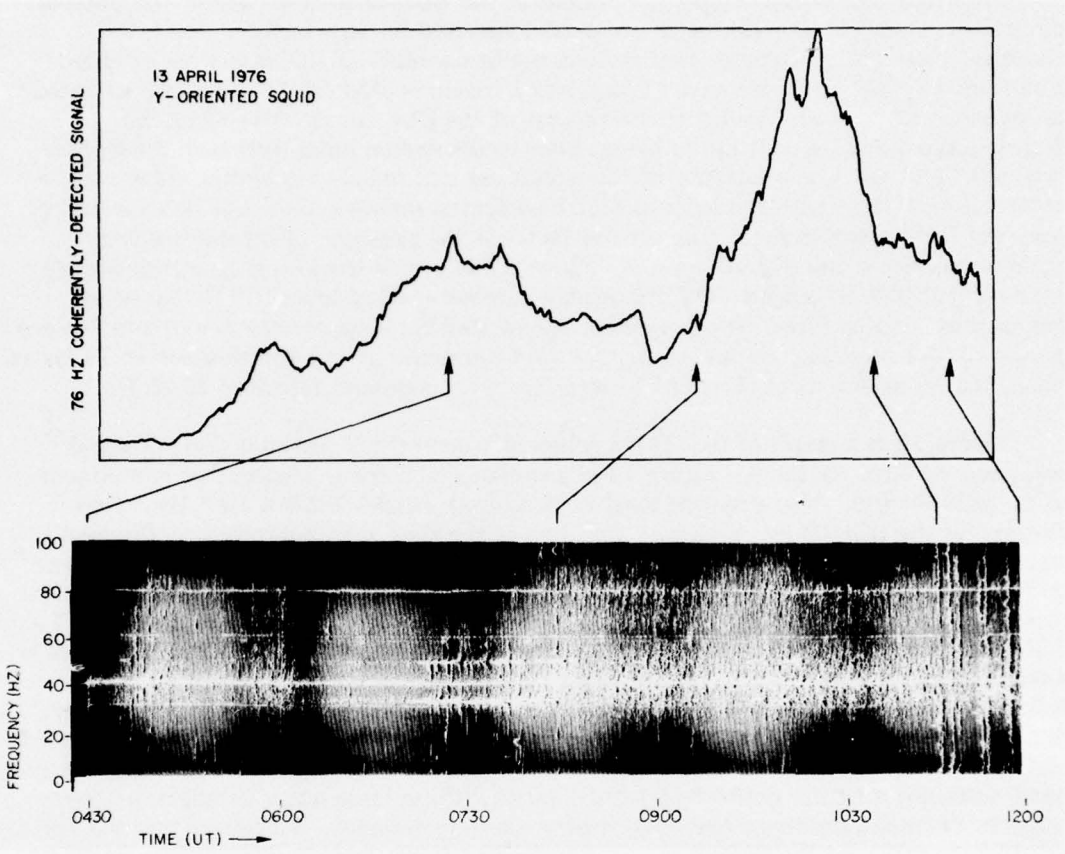

Fig. 12—Comparison of detected ELF signal with spectrum of SQUID output. The trace of the detected ELF signal is also shown in Fig. 13.

During reception of the ELF signal, the output of a synthesizer set to 150 Hz was also recorded on tape. To verify that the 76-Hz signal in Fig. 13 does not simply result from incoherent noise impulses overloading the lock-in detector or from broad-band noise, we used this 150-Hz signal to derive a 75-Hz reference for the lock-in detector. The SQUID outputs were then coherently detected at 75 Hz for comparison with the 76-Hz variation; if a temporal variation were observed at 75 Hz similar to the 76-Hz variation, then interfering broadband noise would be indicated, and this would mean that detection of the broadcast signal had not been achieved. The temporal variation at 75 Hz was found to be characteristic of noise and had an average value of approximately -188 dBH, nearly 16 dB lower than the 76-Hz signal. The value of -188 dBH is higher by about 6 dB than the SQUID system noise level of -196 dBH. This excessive noise probably arises from such diverse sources as the boat-mounted generators, ocean wave-generated noise, and vibration of the antenna in response to cable strumming.

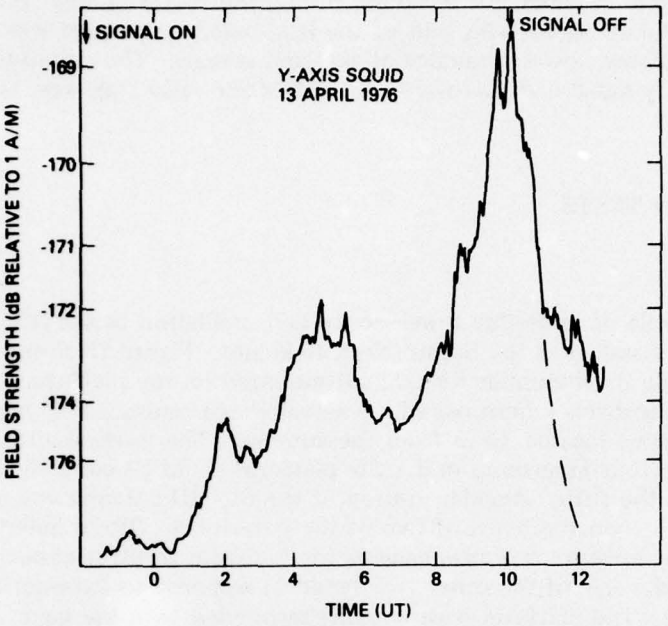

Fig. 13—Transmitted ELF signal received on the bottom-mounted SQUID antenna

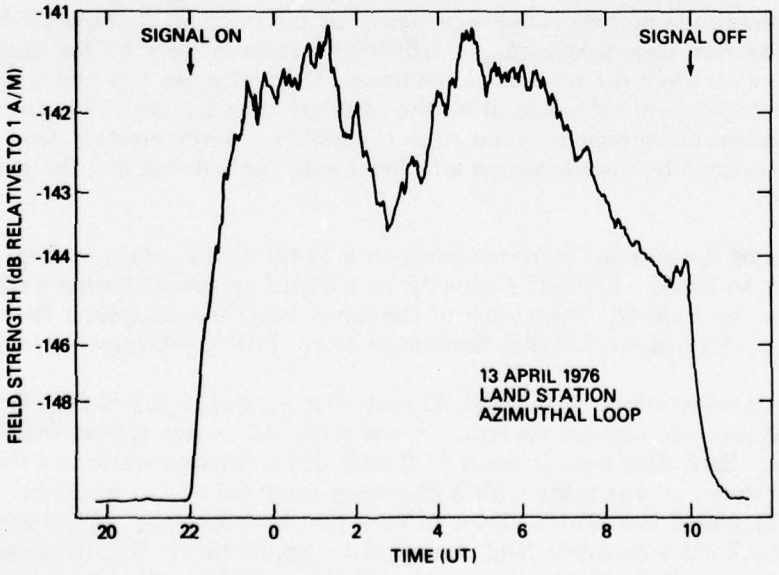

Fig. 14—Transmitted ELF signal received on land station azimuthal loop

Similar results were obtained for reception during the following day, Apr. 14, 1976. Comparison of the SQUID signal with that of the land-based loop signal was not possible because of a failure of the power generator at the land station. The amplitude of the SQUID-detected 76-Hz signal and the overall signal-to-noise ratio were very similar to the Apr. 13, 1976, data.

V. SQUID MOTION TESTS

A. Test Method

A platform capable of imparting a well-controlled oscillation to the SQUID antenna was constructed and installed at the Stump Neck field site. Figure 15 shows the SHE SQUID antenna (inside its aluminum RFI shield) mounted on the platform. The platform rests on four small motorcycle innertubes whose air valves are connected by hoses to the air valve of a fifth innertube located 15 m from the antenna. The internal air pressure, and hence the size, of the four innertubes under the platform could be controlled by applying external force on the fifth. Angular motion of the SQUID antenna was accomplished by putting pinch clamps on the hoses of two of the innertubes. These innertubes maintained a constant pressure and size, causing the platform to pivot about the line joining these two as the size of the other two varied in response to external force on the remote innertube. The platform with antenna responded with the largest vibration amplitude when driven at a frequency of about 1.0 Hz. This resonant frequency could be varied by changing the quiescent air pressure in the innertubes or by adding weight to the platform.

The driving force on the remote innertube was applied by manual pressure. A nearly constant-amplitude motion could be achieved at the resonant frequency. Most measurements, however, were taken using a deliberately random force on the innertube, to simulate more accurately the motion of the buoy. Originally, we had hoped that a triaxial rate gyroscope could be mounted on the platform with the SQUID antenna to obtain an independent measurement of the motion amplitude. Unfortunately, the electrical noise generated by the gyroscope interfered with the antenna and the gyroscopes could not be used.

The outputs of the antenna were recorded on a 12-bit digital tape recorder with a bandwidth of d.c. to 10 Hz. Recording directly on a digital recorder allowed a dynamic range of 66 dB to be achieved. Processing of the tapes, using the algorithms discussed in Sec. II.C, was performed on a Digital Equipment Corp. PDP-11/40 minicomputer.

Two different orientations of the SQUID axes with respect to the Earth's field were employed, and at each orientation the antenna was oscillated in two planes, for a total of four data runs. Each data run consisted of 2 min. of continuous motion of the antenna. A fifth data run was made with a frequency response of d.c. to 50 Hz, to assess the effect of an increased bandwidth. Prior to each run, measurements of the approximate values of the Earth's magnetic field components parallel to the SQUID antenna axes were made using a flux gate magnetometer. These measured values were needed for later comparison with the values deduced by the adaptive processing technique.

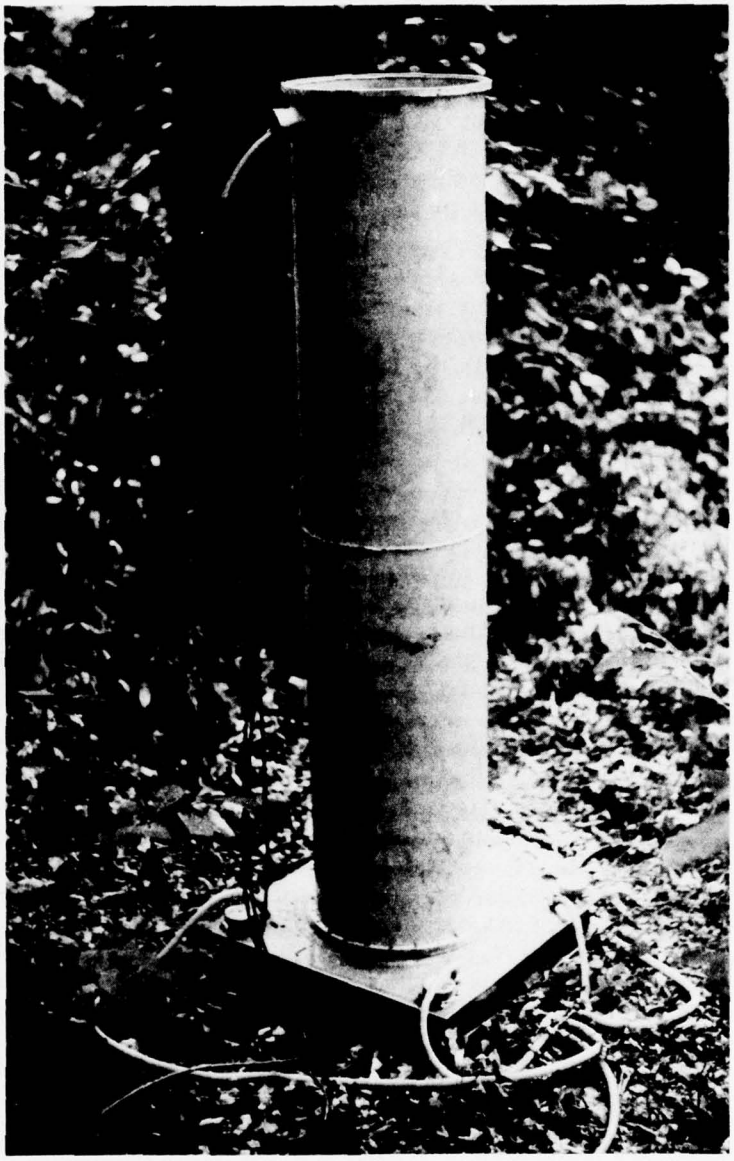

Fig. 15—SHE SQUID (installed in RFI shield) mounted on platform for motion tests

B. Results

The primary goal of the motion tests was to assess the ability of the adaptive processing algorithms to determine the vector **A** in Eq. (2), using actual SQUID outputs. The recorded SQUID outputs were subjected to both the least-squares technique and the steepest-descent technique. Table 7 lists each of the five data runs, identifying them by files and records on the digital tape and giving the parameters of each run. One record corresponds to 331 samples or 3.96 s of data.

1. Least-Squares Technique

An algorithm to invert Eq. (8) to give values of **A** was programed on the PDP-11 computer. The quantity N in Eq. (8), the number of samples, could be made as small as three and as large as the total number of samples in each file. A typical record (converted to analog form) of recorded SQUID outputs is shown in Fig. 15. At time $t = 0$ (the beginning of the record) the three SQUID outputs were zeroed, i.e., the value that each output had at $t = 0$ was subtracted from all subsequent sensor outputs. The values of the A_i subsequently evaluated by the least-squares technique are then appropriate for conditions existing at $t = 0$. As an example of the least-squares computer program results, Table 8 is a listing of the computed values of the components of **A** for records 2 and 3 in file 3. As explained above in connection with Eq. (2), in theory the components of **A** should be approximately equal to the Earth's field components, given in Table 7. It is evident that the computed components of **A**, in addition to having a large degree of scatter, do not agree with the measured values of the Earth's field components. Closer inspection, however, reveals that the *ratios* of the A_i are constant to within about 4%, and these ratios agree with the measured Earth's field component *ratios* to within the experimental errors. This general behavior was observed for all data runs. In Table 9 the ratios of the A_i, as calculated for data from file 3, records 2 and 3, are given for various values of N. The estimate-to-estimate variation in each ratio is given in Table 9 as the standard deviation of the values averaged to obtain the listed ratio. This variation is a measure of the fluctuation or "noise" in the processing. The smallest value of N for which the standard deviation of the ratios assumes its minimum is 75 for A_3/A_2 and 100 for A_1/A_2. These values of N, corresponding to averaging times of 0.9 to 1.2 s, were found to be optimum for many of the records. Further investigation revealed that the optimum N was directly related to the period of oscillation. Figure 16 shows that the period of oscillation in file 3, record 2, is about 1s, correstonding well with the 0.9 to 1.2-s optimum averaging time. In other records, in which the period of oscillation was longer, correspondingly longer averaging times were required. This result is not unexpected: once the motion of the platform has caused the SQUID sensors to sample magnetic field points for one full cycle, further data points are redundant.

The variation in the ratios of the A_i from estimate to estimate, as given by the standard deviation, agrees approximately with the theoretical value, as shown by the following argument. The equation that is evaluated to determine **A** is given by Eq. (2) with $S = 0$ (cf. Eq. (8)). The noise or uncertainty in A_i can be related to the uncertainty in V_i by taking differentials and arriving at the relation $\delta A_i = (A_i/V_i)\delta V_i$. If the ratio $R_{ij} = A_i/A_j$ is defined, it is easy to show that the uncertainty in R_{ij} is given by

Table 7—Parameters for Data Recorded During Motion Tests

Run No.	Tape Identification		Orientation of X-Axis*	Orientation of Rotation Axis*	Measured Field Components (T)†
	File	Records			
Calibration (d.c.)	1	1-30	—	—	—
Calibration (a.c.)	2	1-30			
1	3	1-34	37°E	90°	$H_x = 0.71 \times 10^{-5}$
					$H_y = 0.55 \times 10^{-5}$
2	4	1-33	37°E	0°	$H_z = 2.7 \times 10^{-5}$
3	5	1-27	90°E	90°	$H_x = 5.85 \times 10^{-7}$
4	6	1-32	90°E	0°	$H_y = 0.90 \times 10^{-5}$
5‡	7	1-32	90°E	0°	$H_z = 2.7 \times 10^{-5}$

*With respect to magnetic north.
†Measured with fluxgate magnetometer.
‡Bandwidth increased.

Table 8—Experimental Values of the Components of Vector **A** (Eq. (2)), in $10^{-9}T$, as Determined by the Least-Squares Technique for Two Sample Records

Time (s)	Record No.	Vector **A** Values			Vector **A** Ratios	
		A_1	A_2	A_3	A_1/A_2	A_3/A_2
0.60	2	5808.0	-4280.0	-21870.1	1.357	5.110
1.20	2	11781.2	-8731.2	-44679.9	1.349	5.117
1.80	2	12041.4	-8982.3	-46410.5	1.341	5.167
2.40	2	12232.6	-8744.8	-44621.7	1.399	5.103
3.00	2	10825.5	-7922.8	-40771.0	1.366	5.146
3.60	2	14592.3	-10797.8	-55093.0	1.351	5.102
4.20	2, 3	12556.4	-9258.2	-47579.9	1.356	5.139
4.80	3	6692.9	-4299.2	-22490.1	1.557	5.231
5.40	3	12935.3	-9556.5	-48945.3	1.354	5.122
6.00	3	15348.4	-11399.8	-58181.1	1.346	5.104
6.60	3	10470.7	-7530.4	-38802.3	1.390	5.153
7.20	3	8726.7	-6501.4	-34532.1	1.342	5.311
Average					1.376	5.150
Standard deviation:					0.060	0.062

Note: For file 3, $N = 50$, Averaging time = 0.6 s.

Table 9—Ratios of *A* Components for Various Values of N. The Error Limit on Each Ratio is the Standard Deviation for the Indicated Number of Samples.

N	Averaging Time (s)	Number of Samples	Vector A Ratios	
			A_1/A_2	A_3/A_2
35	0.42	18	1.368 ± 0.1013	4.960 ± 0.447
50	0.60	12	1.376 ± 0.060	5.150 ± 0.062
75	0.91	8	1.350 ± 0.0064	5.114 ± 0.0115
100	1.21	6	1.349 ± 0.0059	5.116 ± 0.0124
150	1.81	4	1.350 ± 0.0062	5.116 ± 0.0131

Note: File 3, Records 2 and 3.

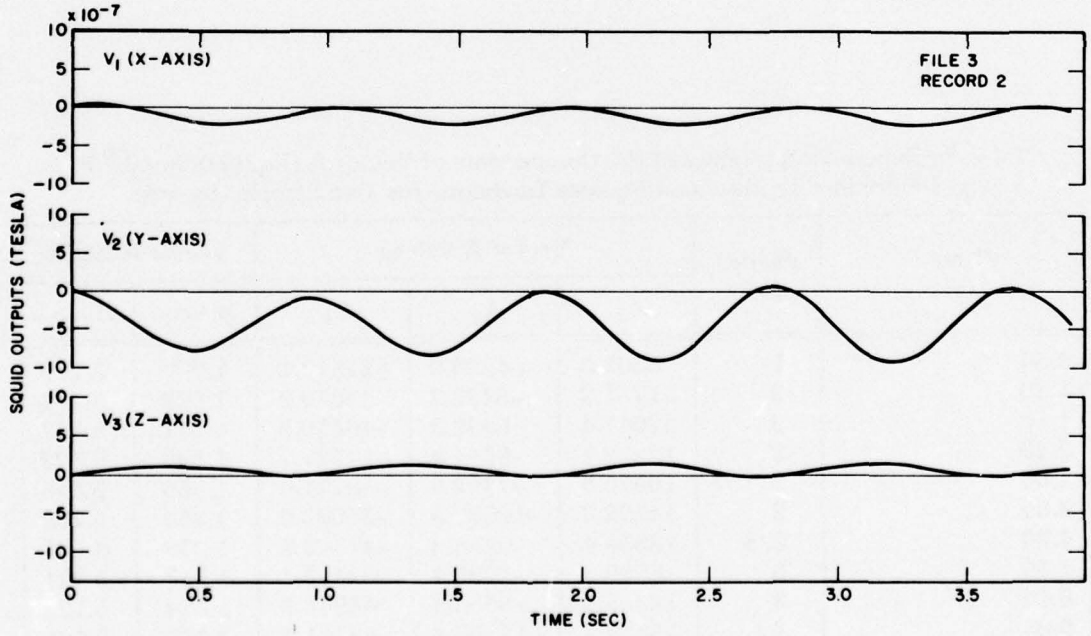

Fig. 16—Example of data recorded during motion tests. Curves have been adjusted to that the amplitude of each is zero at the beginning of the record.

$$\delta R_{ij} = \left(\frac{A_i}{A_j}\right)\left(\frac{\delta V_i}{V_i} - \frac{\delta V_j}{V_j}\right). \tag{13}$$

For simplicity, let us assume that $\delta V_i/V_i = -\delta V_j/V_j = \delta V/V$. (This assumption gives the most pessimistic value of δR_{ij}.) Then

$$\left|\delta R_{ij}\right| \approx 2\left|\frac{A_i}{A_j}\right| \cdot \left|\frac{\delta V}{V}\right|. \tag{14}$$

The value of δV is established in these tests by the noise level of the digital tape recorder, which is 66 dB below the full-scale input of $10^{-6}T$; hence $\delta V = 5 \times 10^{-10}T$. Figure 16 shows that the peak-to-peak value of the variations in the SQUID antenna output for V_1 is approximately $2 \times 10^{-7}T$. Substituting the values of A_i/A_j in Table 9 gives $\delta R_{12} = 0.0068$ and $\delta R_{32} = 0.026$. These values compare reasonably well with the standard deviations listed in Table 9. We conclude that A-D converts with a higher resolution would produce lower fluctuation levels in the computed values of the ratios.

The surprising result of these tests was the inability of the least-squares technique to provide absolute estimates of the A_i. As will be seen in the next section, a similar result was obtained for the steepest-descent processing. A discussion of the reasons for this behavior is deferred until after the steepest-descent processing is presented.

2. *Steepest-Descent Technique*

The complete equation by which each component of **A** is updated is given by

$$A_i(j+n) = A_i(j) - 4K \int_j^{j+n} V_i(t)S(t)dt. \tag{15}$$

The index j refers to the jth sample, and n is the number of integrated points. This equation follows directly from Eqs. (9) and (10). In the implementation of the processing on the PDP-11 minicomputer, the integral was performed by Simpson's rule [14]. As with the least-squares technique, the SQUID outputs were zeroed at $t = 0$, the beginning of the processing.

The performance of the steepest-descent technique was investigated as a function of the parameters K and n in Eq. (15) and $\mathbf{A}_o$, the initial estimate. The quantity K has the nature of a feedback constant; its value determines what fraction of the input signals in the integrand of Eq. (15) is used to correct the current value of A_i. The quantity n determines the number of samples integrated in Eq. (15). This integration functions as a smoothing filter, removing sample-to-sample fluctuations in the V_i. The value of n can be converted to time (seconds) by $t = 0.012n$. An initial estimate $\mathbf{A}_o$ is required to begin the process in Eq. (15).

There are two approaches to the determination of **A** using Eq. (15). The first is to use a fixed length of data and cycle it repetitively through the processing until convergence is obtained. Then, as long as all subsequent data are referenced to the same zero point and the values of the Earth's magnetic field remain constant, the values of A_i determined from this one block of data are appropriate for the subsequent SQUID outputs. We shall refer to this technique as repetitive processing. The second approach is to enter the SQUID's current outputs continuously into the processing, i.e., each sample of the SQUID outputs is processed only once. We shall refer to this technique as sequential processing.

An example of repetitive processing is given in Fig. 17. The processing is begun using initial values of $-1.0 \times 10^{-5} T$ for all components. The fixed data length is one record, or 4 s of data, and the record of data used to generate Fig. 17 is the same as the record displayed in Fig. 16. The quantity n is 5 for this graph, corresponding to an averaging time of 0.06 s. Hence, in each iteration interval, $(4/0.06) \approx 66$ estimates of each A_i are computed. Since the curves in Fig. 17 are drawn through the average value of each A_i during the iteration, large fluctuations in the estimates for the A_i that occur within the first several iterations are not shown. Typically, by approximately the fifth iteration these fluctuations damp out and the estimates of A_i begin to converge monotonically towards the asymptotic value.

The values of A_i to which the curves in Fig. 17 converge are not the values of the Earth's field components. Table 10 lists the values from Fig. 17 to which the curves converge and lists the measured components of the earth's magnetic field (taken from Table 7). It was expected (see the discussion regarding Eqs. (2) and (3)) that these two sets of numbers would show good agreement, but they clearly do not agree. Note, however, that as in the case of the least-squares method, the *ratios* of the asymptotic values in Fig. 17 agree within experimental error with the ratios of the Earth's field components. This behavior was observed, as in the case of the least-squares method, for all of the recorded SQUID outputs processed by the steepest-descent technique.

The effect of the value of feedback constant K on the rate of convergence is shown in Fig. 18. These curves have very nearly an exponential shape beyond the third iteration. By fitting the curves to an exponential equation of the form

$$A = (A_o - A_{\text{asymptotic}})e^{-N/N_o} \tag{16}$$

where N = iteration number, an iteration constant N_o indicative of the rate of convergence of the processing can be derived. Figure 18 indicates that as the value of K increases from $0.2 \times 10^{12}\ T^{-2}$ to $1.5 \times 10^{12}\ T^{-2}$, the value of N_o decreases from 10.7 to 2.6. This convergence rate increase, however, is gained at the expense of a decrease in the stability of the asymptotic value of the A_i. Figure 19 is a plot of N_o and the root-mean-square fluctuation level during the 40th iteration* as a function of K. The fluctuation level is seen to increase rapidly as K is increased above $10^{12} T^{-2}$. For K greater than about $1.6 \times 10^{12}\ T^{-2}$, the process becomes unstable and no convergence is obtained.

*By the 40th iteration, convergence has been obtained for all values of K in Fig. 18.

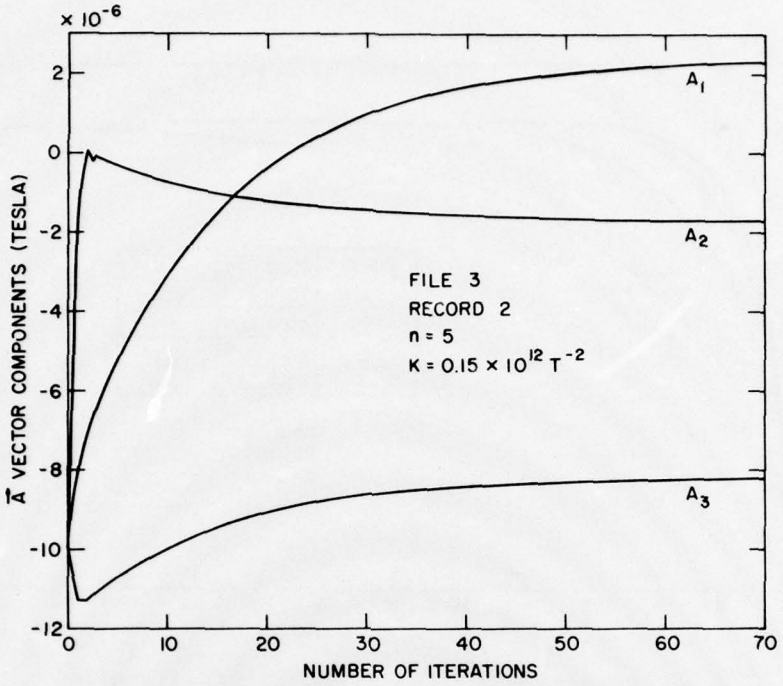

Fig. 17—Convergence curves obtained by using repetitive processing of the record shown in Fig. 16

Table 10—Magnitudes (in $10^{-9}T$) and Ratios of Asymptotic (Convergence) Values of A_i from Fig. 17, Compared to Experimentally Measured Values of the Earth's Magnetic field

Values	Vector A Components			Ratios	
	A_1	A_2	A_3	A_1/A_2	A_3/A_2
Asymptotic (Fig. 17)	2340	-1750	- 8210	-1.34	4.69
Expected (from Table 7)	7100 ±100	-5500 ± 100	-27000 ± 1000	-1.29 ±0.04	4.91 ±0.28

For the data displayed in Fig. 19, a reasonable compromise for a value of K is approximately $0.5 - 10 \times 10^{12}\ T^{-2}$. This range of values for K was also optimum for the remainder of the data recorded during the motion tests. This value of K, interestingly, agrees fairly well with a stability criterion derived by Widrow et al. [15] for adaptive antennas. There is, indeed, a formal similarity between the steepest-descent motion removal technique under discussion here and the adaptive beam-steering technique discussed in Ref. 15. Reference 15 shows that convergence can be obtained when K satisfies

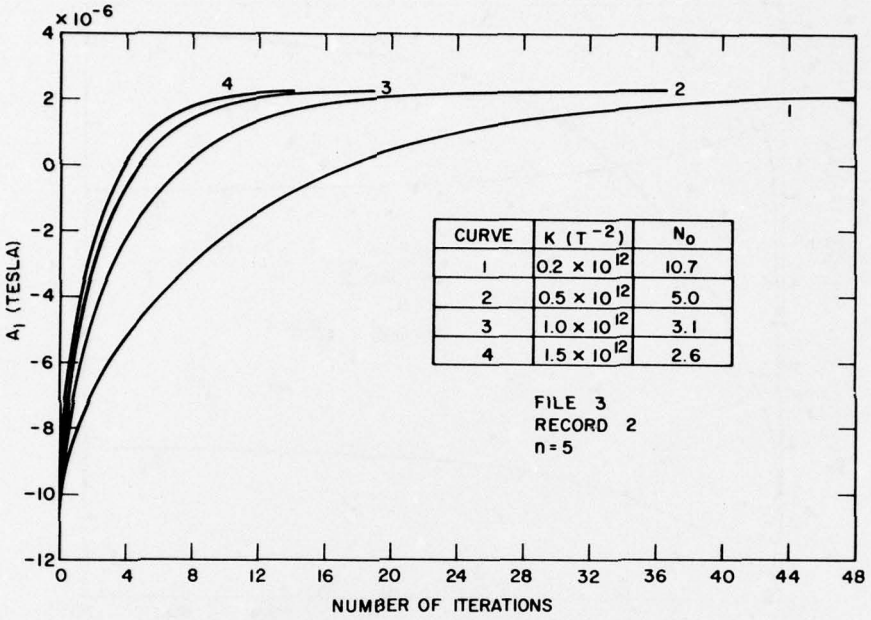

Fig. 18—Convergence curves for A_1, showing the effect of the value of K on the rate of convergence

$$-\frac{1}{P_o} < K < 0 \tag{17}$$

where P_o = total input power. From Fig. 16, the peak-to-peak amplitudes are approximately $2 \times 10^{-7}\,T$, $8 \times 10^{-7}\,T$, and $10^{-7}\,T$, for H_x, H_y, and H_z respectively. Since V_2 leads V_1 by 60 degs and V_3 lags V_1 by 98 deg, the total input power can be estimated as $P_o = 1.2 \times 10^{-13}\,T^2$. Substituting this value of P_o into Eq. (17), we find that K should satisfy

$$-8.3 \times 10^{12} < K < 0. \tag{18}$$

This value of K is of the same order of magnitude as the value $K = -1.6 \times 10^{12}$ found for the onset of stability. The agreement indicates that the processing technique used here behaves in a manner similar to other adaptive systems and suggests that methods employed to improve the characteristics of other adaptive systems might be applied to the motion removal technique.

The behavior of the convergence curves was investigated as n was varied. It was found that for n larger than approximately 10 (corresponding to an integration time of 0.12 s) convergence of the curves was erratic even for the low values of K that normally ensure convergence. Large values of n also resulted in values of the A_i whose ratios did not agree with the ratios of the measured Earth's field components. In general, it appears that the value of n must satisfy the relation

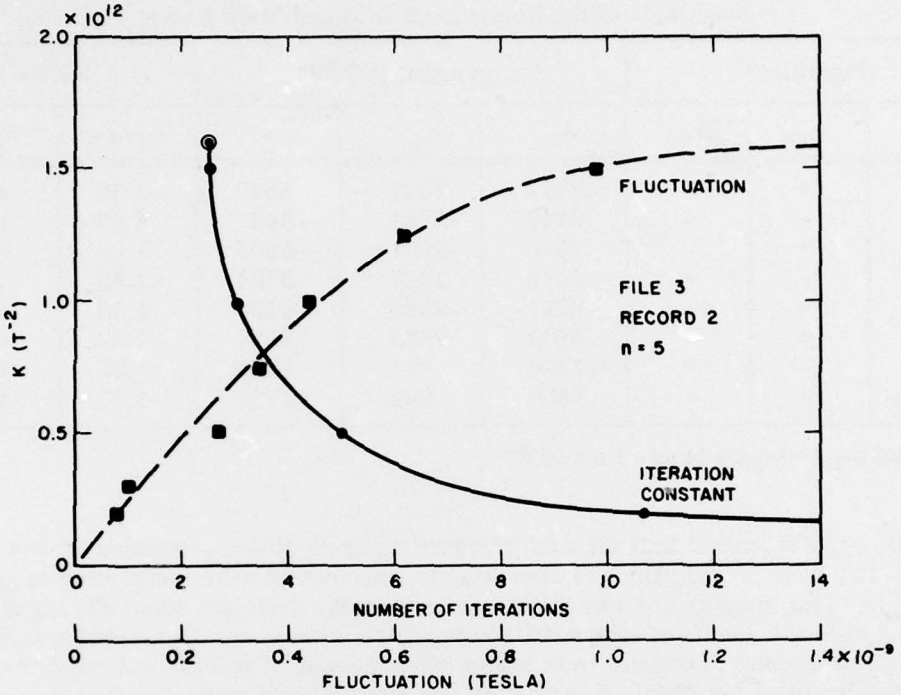

Fig. 19—Effect of the value of K on iteration constant N_O and the RMS fluctuation level of A_1. The circled dot denotes the point at which instability is incipient.

$$n\Delta t \ll T \tag{19}$$

where Δt is interval between samples (0.012 s in this work) and T is the period of the largest motion-induced fluctuations (in this work, usually 1.0 to 2.0 Hz). Intuitively this result follows, because if the averaging time given by $n\Delta t$ becomes an appreciable fraction of the period of the oscillations, then the variations in the SQUID outputs that allow the A_i to be determined are smoothed out. A value of $n = 5$ was used in most of the data processing.

Various combinations of A_{io} were tried, to investigate the dependence of convergence on the initial values. Obviously, as the initial values are made closer to the asymptotic values, the convergence will become faster. The emphasis of the investigation, however, was to determine if the polarities of the initial values had an effect on the achievement of convergence and on the rate of convergence. Table 11 lists the astmptotic values of the A_i for various polarity combinations of the initial values, again for our sample record of file 3, record 2. This table shows that the ratios always attain approximately the same numerical values but that the polarities of the components are either positive A_1, negative A_2, and negative A_3, or the inverse, negative A_1, positive A_2, and positive A_3. Similar results were obtained for all other records investigated in this manner. The implications of this result will be discussed in more detail below.

Table 11—Effect of the Starting Octant of the Initial Values A_{io} on the Sign and Magnitude of the Components of **A** and Their Ratios

Polarities*			Components ($10^{-9}T$)			Ratios	
A_{10}	A_{20}	A_{30}	A_1	A_2	A_3	A_1/A_2	A_3/A_2
+	+	+	-2244	1721	8527	-1.30	4.95
-	-	-	2244	-1721	-8527	-1.30	4.95
+	+	-	2545	-1931	-9504	-1.32	4.92
-	-	+	-2545	1931	9504	-1.32	4.92
+	-	-	3511	-2663	-13104	-1.32	4.92
-	+	+	-3511	2663	13104	-1.32	4.92
+	-	+	-1300	994	4920	-1.31	4.95
-	+	-	1300	-994	-4920	-1.31	4.95

*Note that $|A_{10}| = |A_{20}| = |A_{30}| = 1.0 \times 10^{-5}T$

All results discussed thus far were obtained using repetitive processing of one record. The same investigations of stability and convergence were made using sequential processing. This investigation can be summarized easily: there are essentially no differences between the results of sequential and repetitive processing. Convergence using sequential processing sometimes took longer when a series of records was encountered whose fundamental frequency of oscillation was substantially lower than the typical 1.0 to 2.0-Hz frequency of most records. This was particularily true if these lower frequency oscillations were encountered during the first five or six records of the sequence, when, as Fig. 17 shows, the rate of change of each A_i is fastest. Of course, if one of these records with lower frequency oscillations were used in *repetitive* processing, the convergence would also be slower.

C. Discussion

The inability of either the least-squares or steepest-descent technique to determine the true values of the components of **A** was unexpected. However, it appears that this is a result of the limited dynamic range of the tape recorder. The noise in the first term of Eq. (2), due to the uncertainty δV in **V**, is simply $\mathfrak{N}_1 = 2\mathbf{A} \cdot \delta\mathbf{V}$. The magnitude of $\delta\mathbf{V}$ is given by $\delta V = 10^{-6}\ T/4096 = 2.4 \times 10^{-10}T$, where $10^{-6}T$ is the full-scale amplitude that could be recorded on tape and 4096 is the resolution of the 12-bit A-D converter. Since the magnitude of **A** (if properly evaluated) is $2.8 \times 10^{-5}T$, then $\mathfrak{N}_1 = 3.8 \times 10^{-14}\ T^2$. Now, consider the *amplitude* (as opposed to the noise) of the second term in Eq. (2); taking from Fig. 16, as a typical value, the fields at $t = 0.7$ s gives $\mathbf{V}^2 \approx 2.5 \times 10^{-13}\ T^2$. Note that the amplitude of the second term is only 8 dB above the *noise* of the first term in Eq. (2). Hence, the contribution of the $\mathbf{V}^2$ term to the quantity S in Eq. (2) is close to the system noise level. Indeed, whenever the magnitude of $\mathbf{V}^2$ drops below about $3.8 \times 10^{-14}\ T^2$, the magnitude of the $\mathbf{V}^2$ term descends into the noise level. The consequences of a loss of the information provided by the $\mathbf{V}^2$ term can be determined by reference to Fig. 20. This figure is the same as Fig. 1, except that a plane defined by $\mathbf{A} \cdot \mathbf{V} = 0$ has been added. This plane is a plot of Eq. (2) when the $\mathbf{V}^2$ term is ignored,

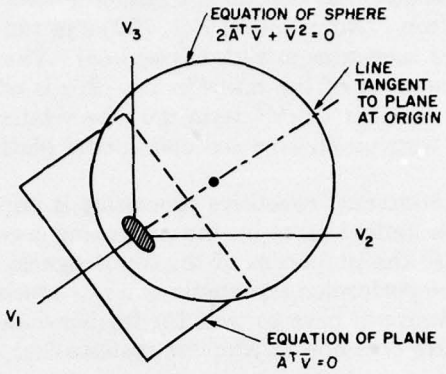

Fig. 20—Geometrical interpretation of Eq. (2) with and without the $\mathbf{V}^2$ term

and is tangent to the sphere at the origin. When the $\mathbf{V}^2$ term in Eq. (2) becomes insignificant due to noise, then the least-squares and steepest-descent techniques attempt to locate the "center" of the plane, not of the sphere. The "center" of the plane is located at a radius of infinity. The best that both techniques can do in this case is to locate the normal to the plane $\mathbf{A} \cdot \mathbf{V} = 0$; this, in fact, is what both techniques do when they correctly evaluate the ratios of the A_i but not the magnitudes.

The highest performance A-D converter available commercially has a resolution of 16 bits. Such an A-D converter would lower the magnitude of $\delta\mathbf{V}$ to $1.5 \times 10^{-11}\ T$ and increase the margin of signal power in the second term in Eq. (2) over noise power in the first term to 20 dB. We believe that this margin would be adequate to allow a unique determination of $\mathbf{A}$. However, we should emphasize that the $\mathbf{V}^2$ term may not be important, and the ratios of the components of $\mathbf{A}$ may be sufficient for the motion noise removal technique. The Appendix in Ref. 10 demonstrates that if the motion noise in the 30-130 -Hz receiver bandwidth is no greater than 2×10^{-5} rad/$\sqrt{\text{Hz}}$, then the $\mathbf{V}^2$ term is not required, i.e., the error introduced by ignoring the $\mathbf{V}^2$ term will be below the system noise level. In Sec. II.B of this report the maximum expected in-band motion noise, on the basis of our towing measurements, is 4×10^{-6} rad/$\sqrt{\text{Hz}}$. Hence, if these measurements eventually prove valid for performance in the ocean under operational conditions, then the $\mathbf{V}^2$ term can indeed be dropped and the ratios of the A_i as evaluated above are sufficient. In this case, Eq. (2) can be written

$$S = \frac{\alpha_1 V_1 + V_2 + \alpha_3 V_3}{\sqrt{1 + \alpha_1^2 + \alpha_3^2}} \tag{20}$$

where $\alpha_1 = (A_1/A_2)$ and $\alpha_3 = (A_3/A_2)$. In place of Eq. (3), the output S is given by

$$S = |H_s|\cos\Psi_s + |H_n|\cos\Psi_n \tag{21}$$

where Ψ_s and Ψ_n are the angles that the Earth's magnetic field makes with the signal and noise vectors, respectively. Note that in Eqs. (20) and (21) S represents a signal voltage rather than a signal power, as in Eqs. (2) and (3). The particular component of **A** chosen for the denominator of the ratios in Eq. (20) is of course arbitrary. The answer to the question of whether the $\mathbf{V}^2$ term must be retained or can be dropped will have to await further tests on an eventual operational platform.

The success of steepest-descent repetitive processing is important, for the convergence rate in this case is limited more by the processing speed of the minicomputer (or microprocessor) than by the properties of the input signals. That is, the processing of one record of data can be performed repeatedly at a rate much faster than real time, and hence the technique does not have to wait for further data to continue convergence. Such speedup techniques are common in adaptive systems (see, for example, Ref. 16).

Figure 21 is a block diagram of a proposed motion noise processor that uses speeded up repetitive processing. The low-pass filtered SQUID signals are digitized and then zeroed, i.e., the value of each SQUID output at a time $t = 0$ chosen arbitrarily as the beginning of the processing is subtracted from all subsequent digitized values. The zeroed digitized values are then entered into the recycling (RC) memory. When this memory is full (4 s of data), the controller commands the repetitive steepest descent processing to begin, using a preset programed value for $\mathbf{A}_o$. The output **A** of the steepest-descent processor is then combined with the high-pass filtered values of **V**. This combiner can form S by either Eq. (2) or Eq. (20), depending on the necessity for retaining the $\mathbf{V}^2$ term. The combiner output is the final SQUID receiver output. This output, however, is continuously monitored; if for any reason the noise increases above some threshold value, the inputs are rezeroed and entered into the RC memory, and the processing begun anew. The apparent noise will increase whenever the components of the Earth's magnetic field change by more than $2.5 \times 10^{-9} T$, the allowable error in the determination of **A** (see the Appendix of Ref. 9). Such changes will occur during large ultralow-frequency fluctuations of ionospheric origin, changes in submarine heading, passage of the sensors near geomagnetic anomalies, and movement through the earth's dipole field gradient. In some cases, particularly changes in submarine heading, the components can vary quite rapidly, and hence fast computation of the A_i (or their ratios) is required.

Table 12 represents an effort to estimate the required computation time. This table assumes the following: (a) the SQUID inputs are digitized at a 30-Hz rate; (b) the integration time is 0.1 s, corresponding to (30 Hz)(0.1 s) = 3 samples per integration; (c) the length of data entered into the RC memory is 4 s, requiring a memory of (3 channels)(30 Hz)(4 s) = 360 points; (d) the processing for each value of A_i is done in parallel; and (e) the $\mathbf{V}^2$ terms have been ignored. The time for each operation, taken from Ref. 17, is appropriate for the Digital Equipment Corp. PDP-11/45 minicomputer using a metal-oxide-semiconductor (MOS) memory. At the optimum value of K, approximately 15 iterations were required to achieve convergence. By Table 12, this implies that a time of 15 (1.37 ms) = 20.5 ms is needed to evaluate **A**. If the $\mathbf{V}^2$ terms are retained, the process time per record is approximately tripled. A considerable savings in computation time can be achieved by using the previous value of **A** as a value of $\mathbf{A}_o$ for the next computation of **A**. This possibility is shown by the dotted line in Fig. 21. It may also prove more advantageous in implementing this technique to eliminate the noise monitoring circuit and continuously update the value of **A**, whether or not reevaluation is actually required.

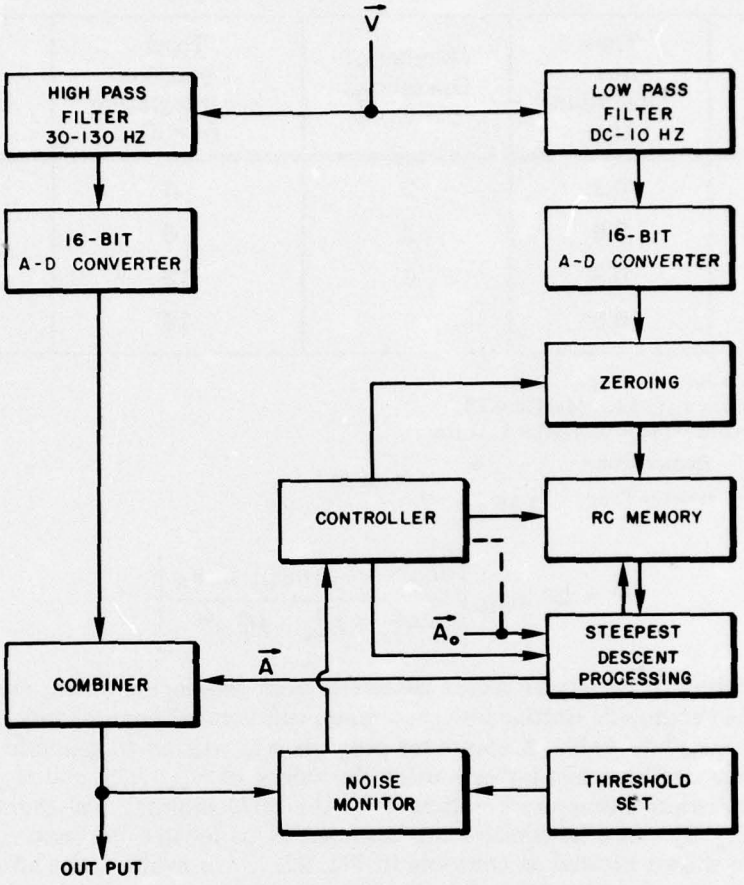

Fig. 21—Proposed motion noise processor

In summary, we believe that the processing technique outlined in Fig. 21, which evolved from our original concept [9] on the baiss of our experimental measurements, is feasible and will achieve the necessary degree of motion noise suppression. Complete verification of the technique will require that a processor operating at a real-time rate be implemented and the broadcast ELF signal be received using this processor while the SQUID is in motion.

D. Effect of Measuring the Signal Projection

As Eq. (3) indicates, the motion noise removal produces an output that is sensitive to the projection of H_s onto the Earth's magnetic field. This circumstance results in an effective decrease in the amplitude of H_s detected by the receiver. This decrease, which we shall denote projection factor F, can be expressed in decibels by the equation

Table 12—Estimate of Repetitive Steepest-Descent Processing Times

Operation	Time per Operation (μs)	Number of Operations per Cycle	Total Operations per Integration ($n = 3$)	Total Time per Integration* (μs)
ADD	0.3	2	6	1.8
MULT	3.6	2	6	21.6
STORE	0.3	6	18	5.4
RECALL	0.3	6	18	5.4

*Time per integration = 34.2 μs
Integrations/record = [(30 Hz)(4s)]/3 = 40
Process time/record = (40)(34.2 μs) = 1.37 ms

$$\text{Speedup factor} = \frac{\text{Record Time}}{\text{Process Time}} = \frac{4}{1.37 \times 10^{-3}} = 2920$$

$$F = 20 \log_{10} \left[\frac{H_{ex} \cos\theta_B + H_{ey} \sin\theta_B}{(H_{ex}^2 + H_{ey}^2 + H_{ez}^2)^{1/2}} \right] \tag{22}$$

where θ_B = bearing of the signal vector measured from geographic north, and H_{ex}, H_{ey}, and H_{ez} are the geographic north-south, east-west, and vertical components, respectively, of the Earth's magnetic field. A computer program was written to generate values of F for points in the northern hemisphere, using the values of H_{ex}, H_{ey}, and H_{ez} given by the standard spherical harmonics coefficients of the 1975 international geomagnetic reference field [18]. The transmitter was assumed to be located in Wisconsin. These values of F are shown plotted as contours in Fig. 22. As is evident, the effective signal amplitude H_s is decreased by 12 to 18 dB in the Norwegian Sea and by 7 to 8 dB in the Mediterranean Sea. In other areas, such as the Pacific Ocean, the decrease is not as severe, averaging 5 to 10 dB.

It is important to note that there is also a decrease in the noise, because the motion noise removal technique also measures the projection of the noise onto the Earth's magnetic field. An exact calculation of the change in signal-to-noise ratio due to projection measurement is of course impossible, since natural ELF noise sources (thunderstorms) are widely distributed and the result will depend critically on the assumed source distribution, strength, model, etc. In general, however, for receiver locations to the north of the principal thunderstorm centers (i.e., north of approximately 45°N latitude), the projection factor is considerably higher for the noise than for the signal, because the noise vector is more nearly perpendicular to the Earth's magnetic field than is the signal vector. Hence, for example, for a receiver located in the vicinity of the Norwegian Sea, the projection factor for a noise source in central Africa is nearly -50 dB, compared to -15 dB for the signal from an ELF transmitter located in Wisconsin. In this example, the signal-to-noise ratio can be expected to improve; however, to take full advantage of such an improvement, the noise level of the SQUID receiver would have to be decreased below $10^{-14} T/\sqrt{\text{Hz}}$.

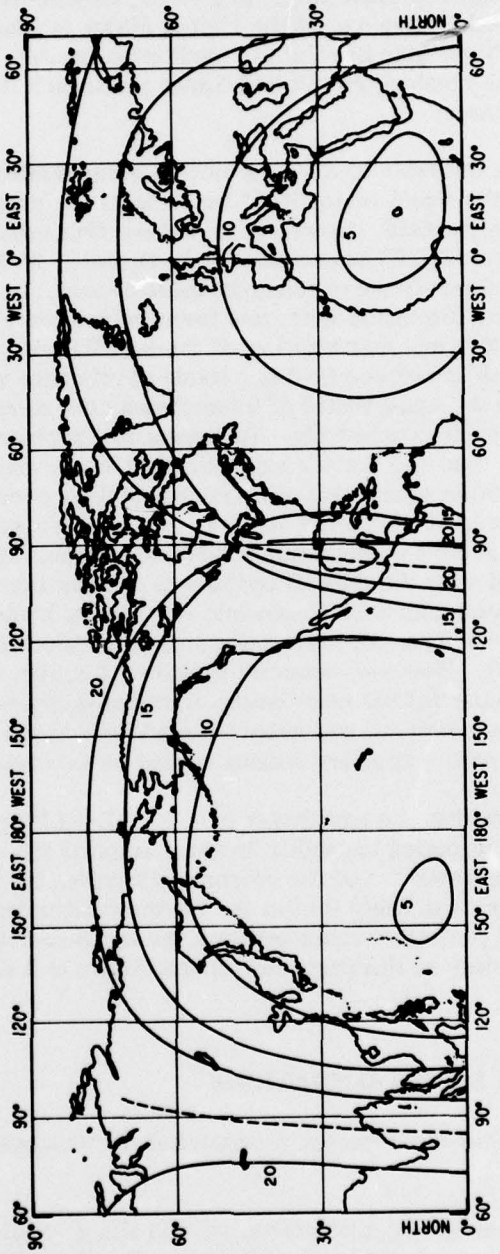

Fig. 22—Contours of projection factor F (Eq. (22)) for the northern hemisphere. The numbers on each contour are values of F in dB below 0 dB. The dashed line is a null.

Changing the transmitter location within the continental United States modifies the contours in Fig. 22, although not drastically. In general, moving the transmitter location towards the western or southern regions of the United States increases the projection factor in areas such as the Norwegian Sea and the Mediterranean Sea. Moving the transmitter location towards the northeastern United States results in a slight decrease in the projection factor in these areas.

It would of course be desirable to devise a motion compensation technique whose output is proportional to the signal vector itself rather than the projection of the signal vector on the Earth's magnetic field. However, we believe that such a technique that uses only the outputs of the SQUID sensors cannot be devised. Motion compensation implies that some stable external frame of reference must be used. In the adaptive motion compensation method under discussion here, this frame of reference is the Earth's d.c. magnetic field. We assert that any combination of the SQUID outputs that attempts to use the direction of the earth's magnetic field as a frame of reference will result in an output sensitive only to changes in the signal vector of interest *along this direction.* We have not, however, proven this statement conclusively. To bypass this problem, it seems clear that a frame of reference other than the Earth's magnetic field would have to be used. There are other approaches to motion compensation. One possibility, considered at length in the early stages of the program, is to use auxiliary rate gryoscopes, accelerometers, or other motion sensors that exploit a gravitational reference frame. The outputs of these sensors would be combined with the SQUID outputs to remove any correlated noise common to the motion sensors and SQUID sensors, which would presumably be a result of motion. One possible technique for performing this correlation adaptively has been given by Widrow et al. [19]. However, concerns regarding the high noise levels of any auxiliary sensors relative to the SQUID noise levels, electrical interference generated by the auxiliary sensors, alinement problems, and simply the added complications from power supplies, signal leads, etc., of the auxiliary sensors caused us to abandon this approach.

In summary, it appears that the advantages of a SQUID ELF receiving antenna are gained at the expense of a degraded capability in some areas of the world because of the projection measurement characteristic of the antenna. However, by decreasing the noise level of the SQUID antenna, it is likely that in the northern latitudes that are affected most seriously by the signal projection characteristics, the signal-to-noise ratio can be raised once more by taking advantage of this projection characteristic as it acts on noise from southerly latitudes.

VI. CONCLUSIONS AND RECOMMENDATIONS

The SQUID ELF receiver development program has demonstrated the following items:

- A horizontal dewar, of an appropriate size and shape to fit in a typical communications buoy, was procured and tested, and demonstrated a 102-day hold time.

- A hydrodynamically stabilized buoy was tested in a towing channel and was fouund to have motion excursions within the 30- to 130-Hz receiver bandwidth that do not exceed 4×10^{-6} rad/$\sqrt{\text{Hz}}$.

- Two test SQUID antennas were procured and evaluated, and both were shown to have sufficient sensitivity, pickup coil orthogonality, linearity, and dynamic range to satisfy all ELF receiver requirements.

- A SQUID antenna received the ELF broadcast signal at a depth of 100 m in the ocean.

- A motion compensation technique was designed and shown using recorded SQUID outputs to be capable of suppressing motion noise to the required degree, when implemented in its final form.

We believe the feasibility of using a triaxial array of SQUID sensors as an ELF submarine receiver has been amply demonstrated by these items. The following additional tasks are necessary, however, before full scale engineering development of an operational ELF receiver can begin.

1. The self-emitted ELF noise should be measured within approximately 300 m of the submarine to determine the required tow cable length and the feasibility of hull mounting.

2. The repetitive processing scheme outlined in Fig. 21 should be implemented with 16-bit A-D converters and a dedicated microporcessor and shown to allow reception of the broadcast ELF signal in real time while the SQUID is in motion.

3. The stabilized buoy that was tested in the DTNSRDC towing basin should be instrumented again with rate gyroscopes and accelerometers and tested in the ocean. These tests can be carried out using a surface craft towing a submerged depressor, to which the buoy is attached by a tow cable of appropriate length.

4. A tow cable that has an integral helium vent line should be procured, and tests of breaking strength, elongation, etc., should be conducted on it.

ACKNOWLEDGMENTS

We are indebted to many people who have assisted us in the various field measurements described in this report. These people include Frederick Belen, William VonFeldt, and Robert Brewer of the David W. Taylor Naval Ship Research and Development Center, Bethesda, Md.; William Brown and Chuck Harris of the Magnetic Test Facility, Goddard Space Flight Center, Greenbelt, Md.; David Cohen and Paul Lawson of the National Magnet Laboratory, Massachusetts Institute of Technology, Cambridge, Mass.; and Michael Cates and Edward Barrett of the Naval Ocean Systems Center (NOSC), San Diego, Calif. We also thank Barry Tossman and Robert Mattey of the Applied Physics Laboratory, Silver Spring, Md., for the use of their pressure vessel during the underwater measurements.

REFERENCES

1. S. A. Wolf, J. R. Davis, and M. Nisenoff, "Superconducting Extremely Low Frequency (ELF) Magnetic Field Sensors for Submarine Communications," *IEEE Trans. Comm.* COM-22, 549-554 (1974).
2. S. A. Wolf, M. Nisenoff, and J. R. Davis, "Superconducting ELF Magnetic Field Sensors for Submarine Communications," NRL Report 7720, May 1974.
3. J. E. Cox, "Potential Cooling Methods for an ELF SQUID," NRL Memorandum Report 2899, Oct. 1974.
4. R. J. Dinger, J. R. Davis, and M. Nisenoff, "Long-Hold-Time Liquid-Helium Dewar for Cooling of a SQUID ELF Antenna," NRL Memorandum Report 3256, Mar. 1976.
5. R. J. Dinger and J. Goldstein, "Motion Stability Measurements of a Submarine-Towed ELF Receiving Platform," NRL Report 7974, Dec. 1975.
6. R. J. Dinger and J. Goldstein, "Motion Stability Measurements of a Submarine-Towed ELF Receiving Platform," *IEEE J. Oceanic Eng.* OE-1, (1976).
7. J. R. Davis, R. J. Dinger, and J. Goldstein, "Development of a Superconducting ELF Receiving Antenna," NRL Report 7990, Apr. 1976.
8. J. R. Davis, R. J. Dinger, and J. Goldstein, "Development of a Superconducting ELF Receiving Antenna," *IEEE Trans.* AP-25 (2), 223-231 (Nov. 1977).
9. R. J. Dinger and J. R. Davis, "Adaptive Methods for Motion-Noise Compensation in Extremely Low Frequency Submarine Receiving Antennas," *Proc. IEEE* 64(10), 1504-1511 (1976).
10. C. W. Sieber, "Full-Scale Demonstrations of the Hydrodynamic Performance of the Primary Towed Vehicle System for Project Classic Thicket," Naval Ship Research and Development Center, Rep. 487-H-02, Oct. 1972.
11. J. G. Park, "The Physics of Resistive SQUIDs Modulated at Low Frequency," *J. Phys. F: Metal Phys.* 4, 2239-2263 (1974).
12. W. L. Goodman, V. W. Hesterman, L. H. Rorden, and W. S. Goree, "Superconducting Instrument Systems," *Proc. IEEE* 61, 20-27, (1973).
13. M. B. Kraichman, *Handbook of Electromagnetic Propagation in Conducting Media*, Naval Material Command, 1970 (AD 714004).
14. R. L. LaFara, *Computer Methods for Science and Engineering*, Hayden Book Co., Rochelle Park, N.J.,
15. B. Widrow, P. E. Mantey, L. J. Griffiths, and B. B. Goode, "Adaptive Antenna Systems," *Proc. IEEE* 55, 2143-2159 (1967).
16. J. F. Meredith and A. J. Dymock, "A Self-Adaptive System Employing High Speed Parameter Identification," in *Proc. 1965 IFAC Conf. Theory* of *Self-Adaptive Control Systems*, P. H. Hammond, ed., Plenum Press, New York, 1966, pp. 165-177.
17. *PDP-11 Processor Handbook*, Digital Equipment Corporation, Maynard, Mass., 1975, p. B-10-B-16.

18. E. H. Vestine, "Main Geomagnetic Field," in *Physics of Geomagnetic Phenomena*, vol. 1, Academic Press, New York, 1967, pp. 181-229.

19. B. Widrow et al., "Adaptive Noise Cancelling: Principles and Applications," *Proc. IEEE*, 63, 1692-1716 (Dec. 1975).